J|A|C|S ARTICLES

Published on Web 12/18/2008

Hydroxynaphthyridine-Derived Group III Metal Chelates: Wide Band Gap and Deep Blue Analogues of Green Alq_3 (Tris(8-hydroxyquinolate)aluminum) and Their Versatile Applications for Organic Light-Emitting Diodes

Szu-Hung Liao,[†,‡] Jin-Ruei Shiu,[†,§] Shun-Wei Liu,[†,||] Shi-Jay Yeh,[†] Yu-Hung Chen,[||] Chin-Ti Chen,*[,†,⊥] Tahsin J. Chow,*[,†] and Chih-I Wu*[,||]

Institute of Chemistry, Academia Sinica, Taipei, Taiwan 11529, R.O.C., Department of Chemistry, National Taiwan Normal University, Taipei, Taiwan 11677, R.O.C., Department of Chemistry and Biochemistry, National Chung Cheng University, Chia-Yi, Taiwan 62102, R.O.C., Graduate Institute of Photonics and Optoelectronics and Department of Electrical Engineering, National Taiwan University, Taipei, Taiwan 10617, R.O.C., and Department of Applied Chemistry, National Chiao Tung University, Hsinchu, Taiwan 30050, R.O.C.

Received September 20, 2008; E-mail: cchen@chem.sinica.edu.tw; tjchow@chem.sinica.edu.tw

Abstract: A series of group III metal chelates have been synthesized and characterized for the versatile application of organic light-emitting diodes (OLEDs). These metal chelates are based on 4-hydroxy-1,5-naphthyridine derivates as chelating ligands, and they are the blue version analogues of well-known green fluorophore **Alq_3** (tris(8-hydroxyquinolinato)aluminum). These chelating ligands and their metal chelates were easily prepared with an improved synthetic method, and they were facially purified by a sublimation process, which enables the materials to be readily available in bulk quantity and facilitates their usage in OLEDs. Unlike most currently known blue analogues of **Alq_3** or other deep blue materials, metal chelates of 4-hydroxy-1,5-naphthyridine exhibit very deep blue fluorescence, wide band gap energy, high charge carrier mobility, and superior thermal stability. Using a vacuum-thermal-deposition process in the fabrication of OLEDs, we have successfully demonstrated that the application of these unusual hydroxynaphthyridine metal chelates can be very versatile and effective. First, we have solved or alleviated the problem of exciplex formation that took place between the hole-transporting layer and hydroxynaphthyridine metal chelates, of which OLED application has been prohibited to date. Second, these deep blue materials can play various roles in OLED application. They can be a highly efficient nondopant deep blue emitter: maximum external quantum efficiency η_{ext} of 4.2%; Commision Internationale de L'Eclairage *x*, *y* coordinates, $CIE_{x,y} = 0.15$, 0.07. Compared with Alq_3, $Bebq_2$ (beryllium bis(benzoquinolin-10-olate)), or TPBI (2,2′,2″-(1,3,5-phenylene)tris(1-phenyl-1*H*-benzimidazole), they are a good electron-transporting material: low HOMO energy level of 6.4−6.5 eV and not so high LUMO energy level of 3.0−3.3 eV. They can be ambipolar and possess a high electron mobility of 10^{-4} cm^2/V s at an electric field of 6.4×10^5 V/cm. They are a qualified wide band gap host material for efficient blue perylene ($CIE_{x,y} = 0.14$, 0.17 and maximum η_{ext} 3.8%) or deep blue 9,10-diphenylanthracene ($CIE_{x,y} = 0.15$, 0.06 and maximum η_{ext} 2.8%). For solid state lighting application, they are desirable as a host material for yellow dopant (rubrene) in achieving high efficiency (η_{ext} 4.3% and η_P 8.7 lm/W at an electroluminance of 100 cd/m^2 or η_{ext} 3.9% and η_P 5.1 lm/W at an electroluminance of 1000 cd/m^2) white electroluminescence ($CIE_{x,y} = 0.30$, 0.35).

1. Introduction

Efficient electroluminescence (EL) was first reported by Tang and Van Slyke using green light-emitting tris(8-hydroxyquinolinato)aluminum (**Alq_3**).[1] Very few materials attract attention as much as **Alq_3** does in organic light-emitting diodes (OLEDs).[2] **Alq_3** has been used as a green emitter, a common electron-transporting material, and a host material for saturated green and red fluorescent dopants.[3] Moreover, due to the rigid ball-like geometry, high glass transition temperature ($T_g \sim 175$ °C),[3c] and polymorphic nature,[4] **Alq_3** is readily sublimed to form amorphous thin films, which is beneficial to the fabrication and operation lifetime of OLEDs. To tune its fluorescence color to

[†] Academia Sinica.
[‡] National Taiwan Normal University.
[§] National Chung Cheng University.
[||] National Taiwan University.
[⊥] National Chiao Tung University.

(1) Tang, C. W.; Van Slyke, S. A. *Appl. Phys. Lett.* **1987**, *51*, 913.
(2) (a) Chen, C. H.; Shi, J. *Coord. Chem. Rev.* **1998**, *171*, 161.
(3) (a) Tang, C. W.; Van Slyke, S. A.; Chen, C. H. *J. Appl. Phys.* **1989**, *65*, 3610. (b) Bulovic, V.; Baldo, M. A.; Forrest, S. R. In *Organic Electronic Materials: Conjugated Polymers and Low Molecular Weight Organic Solids*; Farchioni, R., Grosso, G., Eds.; Springer-Verlag: New York, 2001; p 391. (c) Higginson, K. A.; Thomsen, D. L., III; Yang, B.; Papadimitrakopoulos, F. In *Organic Light-Emitting Devices: A Survey*; Shinar,J., Ed.; Springer-Verlag: New York, 2004; p 71. (d) Chen, C.-T. *Chem. Mater.* **2004**, *16*, 4389.
(4) Brinkmann, M.; Gadret, G.; Muccini, M.; Taliani, C.; Masciocchi, N.; Sironi, A. *J. Am. Chem. Soc.* **2000**, *122*, 5147.

10.1021/ja807284e CCC: $40.75

the red or blue region, some structurally modified **Alq$_3$** derivatives have been developed in past two decades to match the requirement in the RGB full color display or white light illumination application. However, most structurally modified **Alq$_3$** derivatives become less thermally stable and less volatile under reduced pressure. Very often, they fail in the fabrication of OLEDs by a thermal-vacuum-deposition process.

Photophysical and theoretical studies have already provided insight into the electron distribution of the HOMO/LUMO orbitals of **Alq$_3$**.[2,5] Whereas the highest electron density of LUMO is found on pyridine ring, the electrons of HOMO orbitals are located mostly on the phenoxide side of the ligand. An electron-withdrawing substituent on the *para*-position of the phenoxide ring will deplete the HOMO electron density lowering energy level of the filled states. Following the same rationale, the substitution of a electron-donating group on the *para*-position of the pyridine ring will promote the LUMO electron density raising the energy level of the vacant states. Either structural modification results in increasing energy of electrons involved in frontier orbital transition ($\pi-\pi^*$) and an emission that is blue-shifted relative to that of parent **Alq$_3$** (λ_{max}^{f} $\sim$ 514 nm in toluene and 524 in dichloromethane). Although there are several blue or near-blue light-emitting aluminum chelates, **Alq$_3$** derivatives showing deep blue fluorescence (λ_{max}^{f} $<$ 450 nm) have not been realized yet.[2,6] Surveying literature, we have found that a methyl substituent on the pyridine moiety or aza (nitrogen) replacement of "CH" of the phenoxide moiety of **Alq$_3$** is most attractive in blue-shifting fluorescence color, preserving the rigid and globular structure and good valtility of parent **Alq$_3$**. Examples are tris(4-methyl-8-quinolinato)aluminum (**AlmQ$_3$**) and tris(4-[1,5]naphthyridinolato)aluminum (**AlND$_3$**) showing blue-shifted fluorescence at 506 and 440 nm, respectively (Scheme 1). Whereas the greenish **AlmQ$_3$** was reported with EL performance,[6c−f] application of blue **AlND$_3$** for OLEDs is still literature unknown to date.[2] Herein, in addition to the 4-hydroxy-1,5-naphthyridine (**ND**) aluminum chelate, which was efficiently prepared by our improved synthesis, we report the facile synthesis and full characterization of 4-hydroxy-8-methyl-1,5-naphthyridine (**mND**), 2,8-dimethyl-4-hydroxy-1,5-naphthyridine (**mmND**), and 4-hydroxy-2-phenyl-1,5-naphthyridine (**mpND**) metal chelates (Scheme 2). For **mND**, **mmND**, and **mpND** chelating ligands, a whole series of chelates with group III metals (aluminum, gallium, and indium) were also synthesized and characterized. We employ blue-shifting factors of both a methyl substituent and aza (nitrogen element) as the replacement of "CH" in one structure. To our surprise, these metal chelates are in fact new substances and previously unknown. In addition to the thermal stability, they were characterized for deep blue fluorescence and EL in applications of OLEDs. Furthermore, due to their wide band gap and electron-deficient nature, we will demonstrate that these metal chelates are feasible as electron-transporting layer (ETL) material, the host material for highly efficient blue fluorescence dopants, or blue host material for yellow dopants to generate white EL in solid state lighting (SSL) applications.

Scheme 1. Chemical Structures of **Alq$_3$**, **Almq$_3$**, and **AlND$_3$**

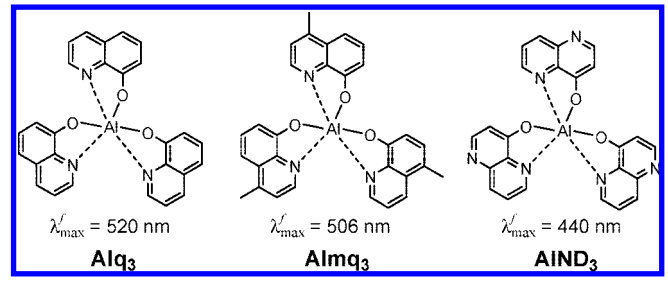

Scheme 2. Chemical Structures of Group III Metal Chelates of 8-Hydroxy-1,5-naphthyridine Derivatives

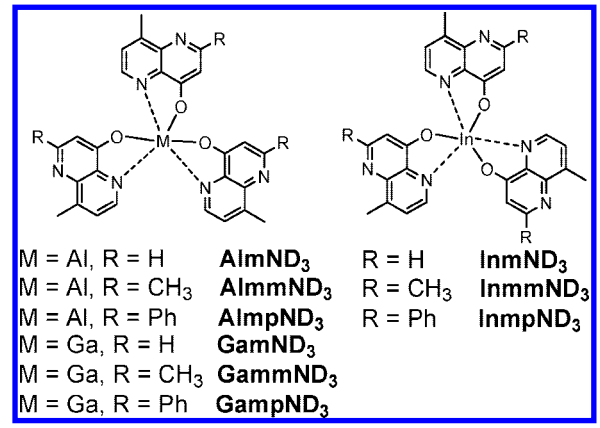

2. Results and Discussion

2.1. Synthesis and Structural Characterization. Parent 4-hydroxy-1,5-naphthyridine (or 1,5-naphthyridin-4-ol) is best known to be prepared by so-called "EMME synthesis" from 3-aminopyridine and diethyl ethoxymethylenemalonate.[7] After the intramolecular cyclization, the hydrolysis of the resulting ester and thermo-decarboxylation of the acid afford 4-hydroxy-1,5-naphthyridine in unsatisfactory overall yields (18−31%).[8] Alternatively, a shorter and more convenient procedure known as the Cassis method in the synthesis of a wide range of 4-1*H*-quinolones (tautomeric forms of hydroxyquinoline) is using

(5) (a) Van Slyke, S. A.; Brynn, P. S.; Levecchio, F. V. U.S. Patent No. 5150006, 1992. (b) Burrow, P. E.; Shen, Z.; Bulvoic, V.; McCarty, D. M.; Forrest, S. R.; Cronin, J. A.; Thompson, M. E. *J. Appl. Phys.* **1996**, *79*, 7991. (c) Sugimoto, M.; Anzai, M.; Sakanoue, K.; Sakaki, S. *Appl. Phys. Lett.* **2001**, *79*, 2348.

(6) (a) Hamada, Y.; Sano, T.; Fujita, M.; Fuji, T.; Nishio, Y.; Shibata, K. *Jpn. J. Appl. Phys.* **1993**, *32*, L514. (b) Hopkins, T. A.; Meerholz, K.; Shaheen, S.; Anderson, M. L.; Schmidt, A.; Kippelen, B.; Padias, A. B.; Hall, H. K., Jr.; Peyghambarian, Armstrong, N. R. *Chem. Mater.* **1996**, *8*, 344. (c) Kido, J.; Iizumi, Y. *Chem. Lett.* **1997**, 963. (d) Kido, J.; Iizumi, Y. *Appl. Phys. Lett.* **1998**, *73*, 2721. (e) Mattoussi, H.; Murata, H.; Merritt, C. D.; Iizumi, Y.; Kido, J. *J. Appl. Phys.* **1999**, *86*, 2642. (f) Sapochak, L. S.; Padmaperuma, A.; Washton, N.; Endrino, F.; Schmett, G. T.; Marshall, J.; Forgarty, D.; Burrows, P. E.; Forrest, S. R. *J. Am. Chem. Soc.* **2001**, *123*, 6300. (g) Yu, J.; Chen, Z.; Sakuratani, Y.; Suzuki, H.; Tokita, M.; Miyata, S. *Jpn. J. Appl. Phys* **1999**, *38*, 6762. (h) Pohl, R.; Anzenbacher, P., Jr. *Org. Lett.* **2003**, *5*, 2769. (i) Pohl, R.; Montes, V. A.; Shinar, J.; Anzenbacher, P., Jr. *J. Org. Chem.* **2004**, *69*, 1723. (j) Montes, V. A.; Li, G.; Pohl, R.; Shinar, J.; Anzenbacher, P., Jr. *Adv. Mater.* **2004**, *16*, 2001. (k) Cheng, J.-A.; Chen, C. H. *J. Mater. Chem.* **2005**, *15*, 1179. (l) Montes, V. A.; Pohl, R.; Shinar, J.; Anzenbacher, P., Jr. *Chem.—Eur. J.* **2006**, *12*, 4523. (m) Pérez-Bolivar, C.; Montes, V. A.; Anzenbacher, P., Jr. *Inorg. Chem.* **2006**, *45*, 9610.

(7) Paudler, W. W.; Kress, T. J. *Adv. Heterocycl. Chem.* **1970**, *11*, 123.

(8) Eck, T. D.; Wehry, E. L., Jr.; Hercules, D. M. *J. Inorg. Nucl. Chem.* **1966**, *28*, 2439.

(9) (a) Cassis, R.; Tapia, R.; Valderrama, J. A. *Synth. Commun.* **1985**, *15*, 125. (b) Chen, B.; Hung, X.; Wang, J. *Synthesis* **1987**, 482. (c) Singh, B.; Laskowski, S. C.; Lesher, G. Y. *Synlett* **1990**, 549. (d) Marcos, A.; Pedregel, C.; Avendaño, C. *Tetrahedron* **1994**, *50*, 12941. (e) Bontemps, N.; Delfourne, E.; Batide, J.; Francisco, C.; Bracher, F. *Tetrahedron* **1997**, *53*, 1743. (f) Kitahara, Y.; Nakahara, S.; Yonezawa, T.; Nagatsu, M.; Shibano, Y.; Kubo, A. *Tetrahedron* **1997**, *53*, 17029. (g) Jeon, M.-K.; Kim, K. *Tetrahedron Lett.* **2000**, *41*, 1943. (h) Salon, J.; Milata, V.; Pronayova, N.; Lesko, J. *Monatch Chem.* **2000**, *131*, 293.

Scheme 3. Synthetic Routes to a Series of 8-Hydroxy-1,5-naphthyridine Metal Chelates

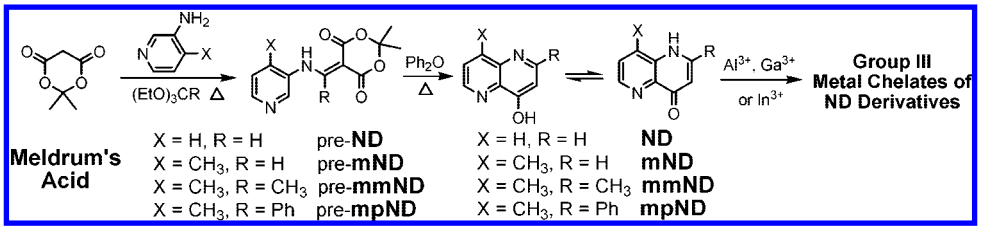

2,2,6-trimethyl-4*H*-1,3-dioxin-4-one (Meldrum's acid) as an effective diketone equivalent precursor.[9] Therefore, we adopted the effective Cassis method in the synthesis of the new naphthyrine derivatives, **mND**, **mmND**, and **mpND** (Scheme 3). For comparison purposes in the study herein, parent chelating ligand **ND** was also synthesized by the more convenient Cassis method.

In the first step of synthesis, four pyridylaminomethylene Meldrum's acid derivatives (pre-**ND**, pre-**mND**, pre-**mmND**, pre-**mpND**) were all obtained in reasonably good yields, 87, 78, 71, and 58%, respectively. Among four species, relatively low yields (58%) of pre-**mpND** can be attributed to the bulky phenyl group that causes sterical hindrance in the formation of the methylene-bridge-head between the amino substituent and Meldrum's acid. In the following step of a ring closure reaction, heating Meldrum's acid derivatives in diphenyl ether afforded **ND**, **mND**, **mmND**, and **mpND** in 47−77% yields, respectively. Among them, **ND** (1,5-naphthyridin-4-ol or 8-hydroxy-1,5-naphthyridine) was obtained in lowest yields (47%), and it is due to formation of an undesired structural isomer (1,7-naphthyridin-4-ol) in the ring closure reaction. The same cause is believed to occur in the previous "EMME synthesis" of **ND**, which was prepared in even lower yields.[8] Nevertheless, the methyl or phenyl substituents of **mND**, **mmND**, or **mpND** are simply from the starting materials of either 3-amino-4-picoline or triethyl orthoacetate/orthobenzoate. A different alkyl group or substituted aromatic ring can be readily incorporated onto **ND** with appropriate starting materials. Through the case of **ND**, it is conceivable that the Cassis method illustrated herein is more convenient and versatile. From the Cassis method, we obtained **ND** in ∼40% overall synthetic yields, which is in fact better than 18−31% overall synthetic yields from the literature reported "EMME synthesis".[8] Moreover, the advantage of the Cassis method is the simpler and more reliable synthetic operation, a two-step procedure instead of a four-step procedure. In "EMME synthesis", a tedious purification process has to be performed four times after each step in the synthetic sequence. The newly synthesized 4-hydroxy-1,5-naphthyridine derivatives were successfully converted into group III metal chelates. However, due to the different reactivity of the metal starting material and the different solubility of the metal chelate product, various reaction conditions and the isolation/purification method were adopted in the final metal chelation reactions, which is somewhat variant from the conventional method preparing **Alq$_3$** (see Experimental Section for details). Basically, the synthesis and purification of hydroxynaphthyridine group III metal chelates are not much difficult than those for the easily prepared and purified **Alq$_3$**. They can be readily obtained with volume production in a conventional synthetic laboratory.

These metal chelates were fully characterized by ^{1}H and ^{13}C NMR, mass spectroscopy, and elemental analysis, and they were consistent with proposed structures. Particularly, a single crystal X-ray structure of **AlND$_3$** was obtained. Its ORTEP drawing is displayed in Figure 1.[10] Similar to that of **Alq$_3$**, the meridional (*mer*) configuration of **AlND$_3$** is clearly evident by the structure diagram and it is consistent with its complicated ^{1}H NMR spectrum. Interestingly, unlike **AlmND$_3$** or **GamND$_3$**, **InmND$_3$** exhibited a simple ^{1}H NMR spectrum (four sharp and well-separated proton resonances), an indication of the facial (*fac*) configuration of **InmND$_3$**. However, recent evidence has demonstrated that the simple ^{1}H NMR spectrum of **Inq$_3$** (and hence **InmND$_3$**) is due to the rapid fluxional transitions between *mer* and *fac* configurations on the NMR time scale.[11]

The higher level of electron deficiency of **ND** than 8-hydroxyquinoline is evident by the significantly smaller pK_a 2.85 of **ND** than pK_a 5.13 of 8-hydroxyquinoline.[12] **ND** derivatives have been known for keto−enol tautomerism in polar organic solvents (see Scheme 3).[7] We found that the extent of naphthyridone tautomeric forms (and hence the pK_a value) can be gauged by the ^{1}H NMR signal (chemical shift) of the proton next to the hydroxy substituent of 8-hydroxyquinoline, **ND**, and **mND**, which locates at 7.09, 6.52, and 6.50 ppm, respectively (see Figure 2). We expect that even smaller pK_a values are present for **mmND** and **mpND**. The smaller pK_a values (due to the electron deficiency) render **ND** derivatives weaker δ-donors on the phenoxide side of the chelating ligand. As the result of a weaker δ-donor, the average Al−O bond distance of **AlND$_3$** (1.867 ± 0.03 Å) is longer than that (1.856 ± 0.02 Å) of **Alq$_3$**.[4] On the pyridine side of the chelating ligand, the average Al−N bond distance of **AlND$_3$** (2.025 ± 0.03 Å) is shorter than that (2.051 ± 0.02 Å) of **Alq$_3$**, and this can be attributed to the "seesaw-like" binding mode of a bidentate chelating ligand. Otherwise, it can be attributed to the stronger N δ-donor in **AlND$_3$** than in **Alq$_3$** because of the electron-donating methyl substituent *para* to the N δ-donor. We believe that the strength of the δ-donor (or the electron deficiency) of chelating ligands is one of the reasons why aluminum metal chelates of **mND**, **mmND**, or **mpND** all have a shorter fluorescence peak wavelength and are better in blue color purity than **AlND$_3$** or **Alq$_3$** (see Table 1 for fluorescence data).

2.2. Photophysical Properties and Energy Levels. Whereas it is the desired deep blue color (λ_{max}^{fl} 415−417 nm) of **AlmND$_3$**, **AlmmND$_3$**, and **AlmpND$_3$**, a less satisfactory sky blue fluorescence (λ_{max}^{fl} 433 nm) of the previously known **AlND$_3$** is clearly shown in their solution fluorescence images (see Figure 3). In the solid state, all four aluminum chelates display red-shifted fluorescence wavelength λ_{max}^{fl} 425 nm (**AlmpND$_3$**), 431

(10) Crystal data for **AlND$_3$**·CH_2Cl_2: $C_{25}H_{17}AlCl_2N_6O_3$: Fw = 547.33, Triclinic, $P\bar{1}$, Z = 2, $F(000)$ = 560. Cell dimendions: a = 7.9946(7) Å, b = 12.0879(11) Å, c = 13.1153(12) Å, α = 70.346(2)°, β = 82.950(2)°, γ = 84.082(2)°, V = 1181.98(18) Å^3, $2\theta_{max}$ = 50.0°, ρ_{cacld} = 1.538 mg/m^3. Of 8777 reflections, 4157 were independent, 334 parameters, $R(F_o)$ = 0.0588 (for reflections with $I > 2\sigma(I)$), $R_w(F_o)$ = 0.1663 (for reflections with $I > 2\sigma(I)$). The GoF on F^2 was 0.977.

(11) Sapnochak, L. S.; Ranasinghe, A.; Kohlmann, H.; Ferris, K. F.; Burrows, P. E. *Chem. Mater.* **2004**, *16*, 401.

(12) Mason, S. F. *J. Chem. Soc.* **1957**, 5010.

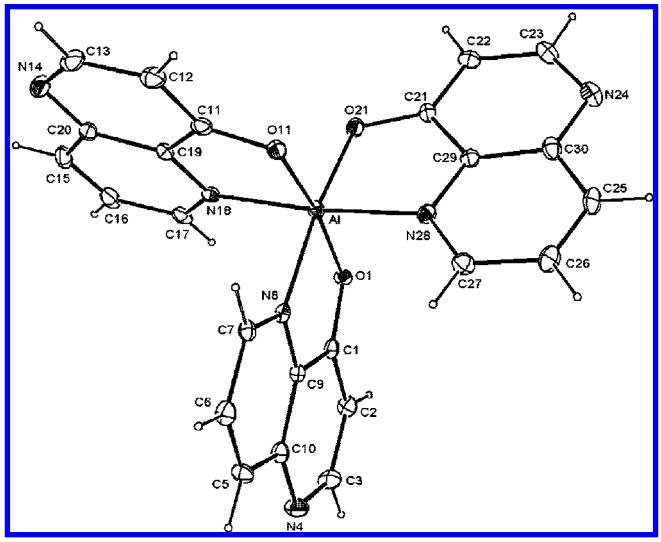

Figure 1. Molecular structure of **AlND$_3$** determined by X-ray diffraction analysis.

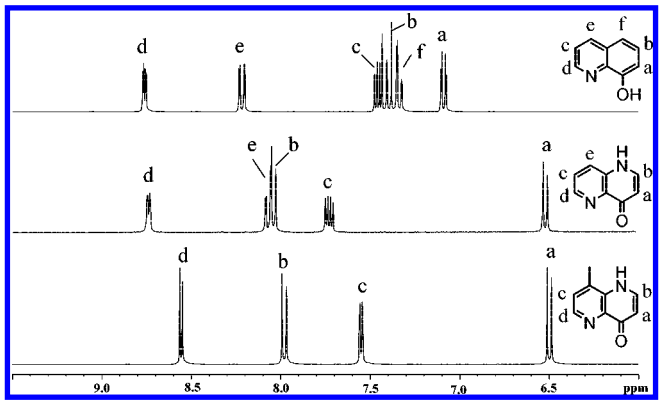

Figure 2. ^{1}H NMR spectra of 8-hydroxyquinoline, **ND**, and **mND** in CD_3OD from top to bottom, respectively.

Table 1. Optical and Thermal Properties of Metal Chelates of 4-Hydroxy-1,5-naphthyridine Derivatives

	solution[a]			solid					
metal chelates	λ_{max}^{ab}, $\lambda_{on\ set}^{ab}$ (nm)	λ_{max}^{fl} (nm)	Φ_f (%)	λ_{max}^{fl} (nm)	Φ_f (%)	T_g (°C)	T_c (°C)	T_m (°C)	LUMO/HOMO (eV)[b]
Alq$_3$	388, 443	524	20	516	40	174	367	412	3.1/5.9
AlND$_3$	341, 381	433	47	447	45	122	262	412	-
AlmND$_3$	338, 370	415	45	431	43	196	277 387	420	3.0/6.4
AlmmND$_3$	335, 372	416	45	419	39	233	[c]	436	-
AlmpND$_3$	326, 376	417	45	425	6	204	278	370	-
GamND$_3$	341, 374	431	45	439	41	[c]	[c]	414	3.2/6.5
GammND$_3$	339, 376	432	42	434	52	212	[c]	430	-
GampND$_3$	327, 383	432	25	439	11	185	275	381	-
InmND$_3$	344, 382	436	37	445	12	183	[c]	361	3.3/6.5
InmmND$_3$	332, 381	437	36	436	22	221	[c]	372	-
InmpND$_3$	329, 386	437	23	446	8	186	224	370	-

[a] In dichloromethane. [b] HOMO energy was determined as the edge of HOMO energy level or the ionization potential of the material; LUMO energy was determined as the lowest photoexcitation state energy from the on-set absorption energy in absorption spectra. [c] Not observed.

nm (**AlmND$_3$**), and 447 nm (**AlND$_3$**), except λ_{max}^{fl} 419 nm of **AlmmND$_3$** (Table 1). In dichloromethane solution, all four aluminum chelates have reasonably good fluorescence quantum yields (Φ_f) around 45−47% but more or less suffer from fluorescence concentration quenching in the solid state (Table 1).

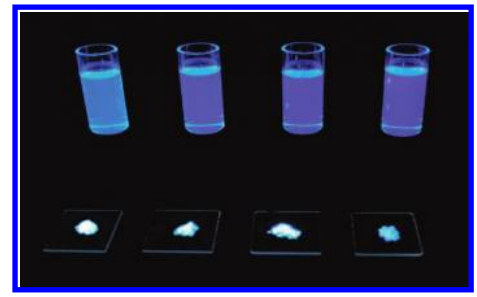

Figure 3. Solution (in dichloromethane) and solid state fluorescence image of **AlND$_3$**, **AlmND$_3$**, **AlmmND$_3$**, and **AlmpND$_3$** from left to right, respectively.

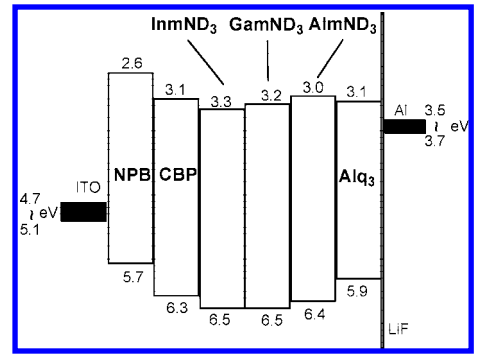

Figure 4. Energy alignment of **AlmND$_3$**, **GamND$_3$**, **InmND$_3$**, **Alq$_3$**, NPB, and CBP in OLED devices based on ITO anode and LiF/Al cathode.

Among them, **AlmpND$_3$** has the most severe fluorescence quenching in the solid state with a Φ_f of only 6%. Such solid-state fluorescence quenching is universal for **mpND**-based chelates (**AlmpND$_3$**, **GampND$_3$**, and **InmpND$_3$**. This can be rationalized by the molecular contact (probably $\pi-\pi$ interaction) through protruded phenyl substituents in the solid state. With no exception of the three chelating ligands **mND**, **mmND**, and **mpND**, fluorescence of these metal chelates was observed to be reduced with increasing atomic number of the metal ion from Al to Ga and then In (see Φ_f data in Table 1), known as the heavy atom effect that increases in the rate of intersystem crossing.[2,13]

In the search for the origin of the wide band gap nature, **AlmND$_3$**, **GamND$_3$**, and **InmND$_3$** were found to have a HOMO energy level around 6.4−6.5 eV, which is significantly lower than 5.9 eV of **Alq$_3$** (Figure 4). The LUMO energy level of three **mND** metal chelates is around 3.0−3.3 eV, which is similar to or just a bit lower than 3.1 eV of **Alq$_3$**. This is perfectly logical because the prominent electron deficient feature (N aza substituent) locates on the HOMO of the molecule, which is the pyridin-4-olate ring of the chelating ligand, instead of the LUMO of three **mND** metal chelates, which is the *para*-methylpyridine (or 4-picoline) ring of the chelating ligand. It can be further identified that either HOMO or LUMO is stabilized by the higher atomic number of the central metals, Al, Ga, and In. Such a stabilization effect happens more prominently in the LUMO than in the HOMO. As a result, the energy band gap of three **mND** metal chelates decreses in the order **AlmND$_3$** > **GamND$_3$** > **InmND$_3$**. Relative to that of **Alq$_3$**, a significantly low HOMO energy level and moderately low LUMO energy level enlarge the energy band gap of these hydroxylnaphthyridine-based metal chelates.

(13) Burrow, P. E.; Sapochak, L. S.; McCarty, D. M.; Forrest, S. R.; Thompson, M. E. *Appl. Phys. Lett.* **1994**, *64*, 2718.

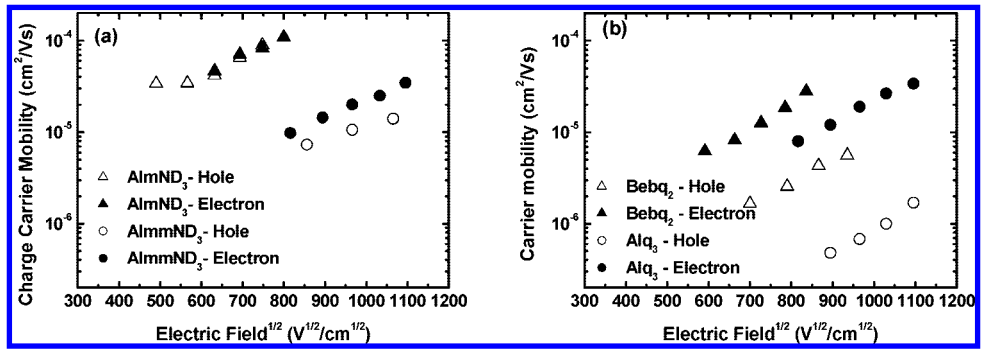

Figure 5. Hole and electron mobility vs the square root of the applied electric field of **AlmND$_3$** and **AlmmND$_3$** (a) and Alq$_3$ and Bebq$_2$ (b).

2.3. Charge-Transporting Properties and Charge Carrier Mobilities. In terms of HOMO and LUMO energy levels, hydroxynaphthyridine-based metal chelates are better hole-blocking or electron-transporting materials than **Alq$_3$** or other deep blue fluorophores. Most known deep blue fluorophores are based on triarylamines, such as NPB, or nonheteroatom-containing polycyclic aromatic hydrocarbons (PAHs), such as anthracene, perylene, pyrene, or spirobifluorene compounds. Compared with those of hydroxynaphthyridine metal chelates, such nonmetal chelate deep blue fluorophores have significantly higher HOMO and LUMO energy levels of 5.1−5.8 eV and 2.0−2.7 eV (assuming band gap energy is ca. 3.1 eV) below vacuum level, respectively.[14]

The HOMO−LUMO energy level of the material shown above is one of the determining factors for electron-transporting or hole-transporting properties of OLED materials. The charge carrier (electron or hole) mobility is the other decisive characteristic that influences the charge-transporting nature and hence the efficiency performance of OLEDs. The relative magnitude of the electron and hole mobility of the material indicates the extent of charge balancing, the efficiency of charge recombination, and hence the EL efficiency of OLEDs. We measured the intrinsic charge carrier (hole or electron) mobility in a bulk film (0.6−1 μm) of **AlmND$_3$** and **AlmmND$_3$** using the optical time-of-flight (TOF) technique that has been described before. In addition, we also took a measurement on **Alq$_3$** and Bebq$_2$ with the same measuring system for comparison and accuracy checking. Figure 5 shows the field dependence of the hole and electron drift mobility of **AlmND$_3$**, **AlmmND$_3$** (Figure 5a), **Alq$_3$**, and Bebq$_2$ (Figure 5b). First, the electron mobility of **Alq$_3$** was determined to be $\sim 10^{-5}$ cm^2/V s at an electric field of 6.4 $\times$ 10^5 V/cm, which agrees with those obtained previously.[15] Second, the electron mobility of Bebq$_2$ was determined to be $\sim 10^{-4}$ cm^2/V s at the same electric field, which is 1 order of magnitude higher than that of **Alq$_3$** and consistent with the report that Bebq$_2$ is a better electron-transporting material than **Alq$_3$**.[16] Devices with an electron-transporting layer (ETL) of Bebq$_2$ have been demonstrated with lower driving voltage and longer operation lifetime, when compared with ones with **Alq$_3$** as an ETL.[16] Third, we found that the charge carrier (either hole or electron) mobility of **AlmND$_3$** is higher than that of **AlmmND$_3$** by nearly 1 order of magnitude (Figure 5a). In fact, checking the extrapolated data in the range of electric field of (3.6−6.4) $\times$ 10^5 V/cm, the charge carrier (either hole or electron) mobility of **AlmND$_3$** is the highest among all (Figure 5a and 5b). Therefore, **AlmND$_3$** is probably a better electron-transporting material than **AlmmND$_3$** because of its high electron mobility. In addition, **AlmND$_3$** seems to be the only material that is ambipolar because of its very similar hole and electron mobility determined by TOF technique. On the other hand, **AlmmND$_3$** may be a better nondopant deep blue emitter because of its low hole mobility, which limits the amount of hole carrier on **AlmmND$_3$** and enhances the charge balance in normally hole-dominated devices, one crucial factor for high efficiency OLEDs. As shown in the following sections (**2.7** and **2.8**), our OLED results are consistent with the forgoing derivation from the TOF data of **AlmND$_3$** and **AlmmND$_3$**.

2.4. Thermal Properties. Figure 6 shows the differential scanning calorimetry (DSC) thermograms of **Alq$_3$**, **AlND$_3$**, **AlmND$_3$**, **GamND$_3$**, **AlmmND$_3$**, and **GammND$_3$**. In DSC measurements, these metal chelates were first taken from the sample that was purified by a sublimation process. With such prethermal-annealed samples (sublimed-scarped samples), we found that DSC thermograms often show nothing but weak endothermic step transitions, indicative of the glass phase transition temperature (T_g). To reveal DSC signals of other phase transition temperatures, such as crystallization temperature (T_c), melting temperature (T_m), or polymorphic phase transition temperature (T_p), the sublimed-scarped samples of metal chelates were redissolved in dichloromethane and then evaporated until dryness under reduced pressure at room temperature. In Figure 6, each metal chelate is displayed with two types of DSC traces. First the heating scan, positioned as the top scan, has a heating temperature beyond the large endothermic signal, T_m. The other scans marked with the sequence number of heating scans or cooling scans in Figure 6 are DSC traces with a measuring temperature less than T_m, except for **AlmpND$_3$**, **GampND$_3$**, and **InmpND$_3$** (see Figure S1 for their DSC traces). Two types of heating thermograms were displayed because these metal chelates often exhibit thermal decomposition right after their melting transition, which was evident from observations from a polarized optical microscope (POM). With samples prepared under such conditions, **Alq$_3$** shows T_g (on-set T_g) at 174 °C, a broad and small endortherm peaking at ~355 °C (assigned as T_p) immediately followed by an exotherm peaked at 367 °C (T_c), and finally a large endothermic signal at 412 °C (T_m). Whereas a T_g of 174 °C and T_m of 412 °C are rather consistent with literature data for **Alq$_3$**,[3c,4,6f,17] the coupled endortherm and

(14) Adachi, C.; Oyamada, T. *Data Book on HOMO Levels of Organic Thin Films in Organic Semiconductor Devices*; CMC Publishing: Tokyo, 2005.
(15) Tse, S. C.; Kwok, K. C.; So, S. K. *Appl. Phys. Lett.* **2006**, *89*, 262102.
(16) (a) Lee, J.-H.; Wu, C.-I.; Liu, S.-W.; Huang, C.-A.; Chang, Y. *Appl. Phys. Lett.* **2005**, *86*, 103506. (b) Lee, J.-H.; Ho, Y.-H.; Lin, T.-C.; Wu, C.-F. *J. Electrochem. Soc.* **2007**, *154*, J226.
(17) Higginson, K. A.; Zhang, X.-M.; Papadimitrakopoulos, F. *Chem. Mater.* **1998**, *10*, 1017.

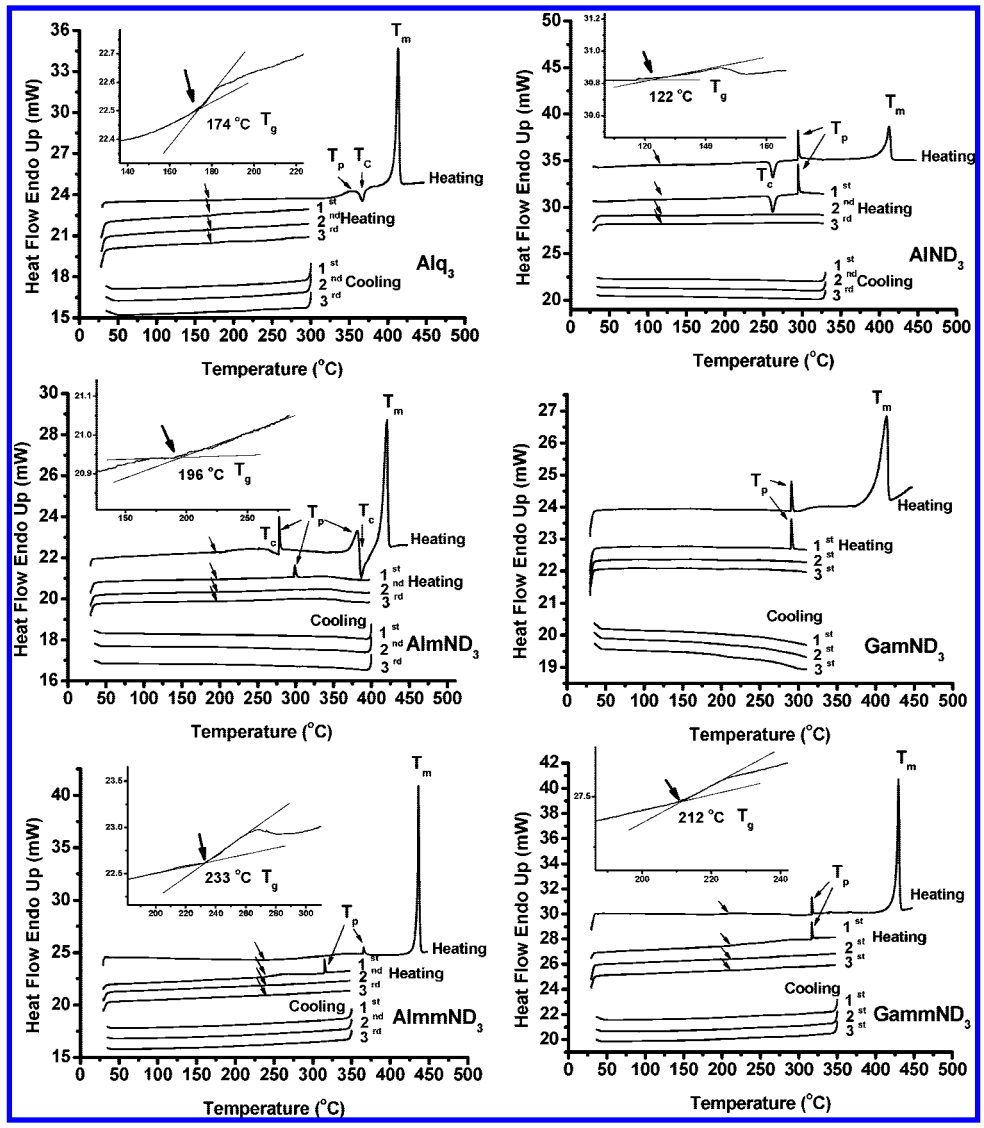

Figure 6. DSC thermograms of **Alq_3**, **$AlND_3$**, **$AlmND_3$**, **$GamND_3$**, **$AlmmND_3$**, and **$GammND_3$**.

exotherm have been shown before, although they were reported at higher temperatures of 393 and 396 °C, respectively.[4,6f,18] It is interesting to know that **Alq_3** will be vaporized (sublimed) when heated around melting temperatures at atmospheric pressure.[6f] We have a similar observation (under POM) for **Alq_3** and most metal chelates reported herein as well. Such an observation is indirect evidence that these new metal chelates preserve their superior volatility as well as **Alq_3**. Unlike those structurally modified **Alq_3** blue derivatives, volatile hydroxynaphthyridine metal chelates reported herein have no problem in the fabrication of OLED by thermal-vacuum-deposition processes.

Alq_3 has been well-known for its polymorphic and racemic nature and its multiple phase transitions that have been studied in great detail recently.[4,6f,18] It has been suggested that the exotherm observed for **Alq_3** in DSC traces is due to crystallization, indicative of the instability of the glassy phase of **Alq_3**. Some new hydroxynaphthyridine metal chelates, such as **$AlmmND_3$**, **$GamND_3$**, **$GammND_3$**, **$InmND_3$**, and **$InmmND_3$**, show no discernible exotherm in DSC traces, a good sign of the morphological stability of their glassy phase. Except for **$AlND_3$** (T_g ~122 °C) and **$GamND_3$** (no detectable T_g in DSC traces), all metal chetates reported herein show T_g values around 183−233 °C, which is higher than 174 °C for **Alq_3** (Table 1). Higher T_g's of metal chetates often imply a higher morphorlogical stability or a glass phase stability, which is beneficial to the operation lifetime of the multiple-thin-film OLEDs. Furthermore, for all aluminum chelates but **$AlmpND_3$**, higher melting temperatures than **Alq_3** were observed by DSC (Table 1). This is a plus because the melting transition of these aluminum chelates was rapidly followed by the thermal decomposition. A higher melting temperature means a higher thermal stability in the case of the aluminum chelates studied herein.

Metal chelates based on **mpND** are different from the rest. Among all metal chelates, **$AlmpND_3$**, **$GampND_3$**, and **$InmpND_3$**

(18) (a) Sano, K.; Kawata, Y.; Urano, T. I.; Mori, Y. *J. Mater.Chem.* **1992**, *2*, 767. (b) Braun, M.; Gmeiner, J.; Tzolov, M.; Cölle, M.; Meyer, F. D.; Milius, W.; Hillebrecht, H.; Wendland, O.; von Schütz, J. U.; Brütting, W. *J. Chem. Phys.* **2001**, *114*, 9625. (c) Cölle, M.; Gmeiner, J.; Milius, W.; Hillebrecht, Bï; utting, W. *Adv. Funct. Mater* **2003**, *13*, 108. (d) Muccini, M.; Loi, M. A.; Kenevey, K.; Zamboni, R.; Masciocchi, N.; Sironi, A. *Adv. Mater.* **2004**, *16*, 861. (e) Levichkova, M. M.; Assa, J. J.; Frob, H.; Leo, K. *Appl. Phys. Lett.* **2006**, *88*, 201912.

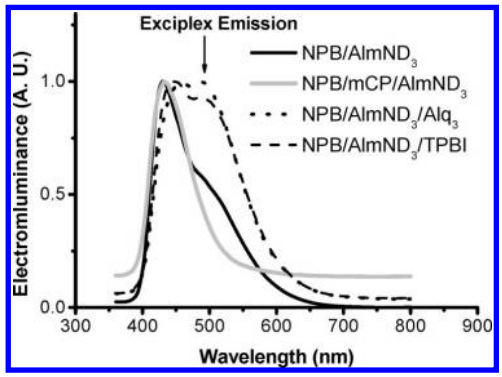

Figure 7. EL spectra of four NPB/**AlmND$_3$**-containing OLEDs: ITO/multiple organic layers/LiF/Al.

were found with relatively low T_g's of 185−204 °C, and they are easily recognizable in repeated heating scans in DSC measurements (Figure S1). Their T_g's were always observed prior to a cold crystallization peak without discernible polymorphic phase transition signals (as T_p marked for **AlND$_3$**, **AlmND$_3$**, and **AlmmND$_3$** in Figure 6). **AlmpND$_3$**, **GampND$_3$**, and **InmpND$_3$** are also a few exceptions that they do not decompose following the melting transition. Such a difference in thermal properties of **mpND**-based metal chelates can be all attributed to the protruded phenyl substituent on a symmetric and nearly globular structure of naphthyridinolate metal chelates.

2.5. Elimination of Adverse Exciplex Formation in Non-Doped Blue OLEDs. Deep blue fluorescence of **AlmND$_3$** or **AlmmND$_3$** is very attractive for highly demanding blue OLEDs. A simple nondoped bilayer EL device ITO/NPB(30 nm)/**AlmND$_3$**(30 nm)/LiF(5 nm)/Al (150 nm) was first fabricated by sequential thermal-vacuum-deposition of NPB, **AlmND$_3$**, LiF, and Al onto ITO (indium tin oxide)-coated glass substrate. Unfortunately, in addition to the emission band peaking around 430−450 nm of **AlmND$_3$**, a pronounced emission band around 480−540 nm appears in the EL spectrum of the device (Figure 7).

Such a long wavelength EL devastates the EL efficiency and also impairs the blue color purity of OLEDs. A similar observation was also found for **AlmmND$_3$** OLEDs. To clarify the origin of the long wavelength EL, three more control devices were then fabricated: ITO/NPB (30 nm)/*m*CP(30 nm)/**AlmND$_3$**(30 nm)/LiF(5 nm)/Al(150 nm), ITO/NPB(30 nm)/**AlmND$_3$** (30 nm)/**Alq$_3$**(30 nm)/LiF(5 nm)/Al(150 nm), and ITO/NPB(30 nm)/**AlmND$_3$** (30 nm)/TPBI (30 nm)/LiF (5 nm)/Al (150 nm). From their EL spectra (Figure 7), we can firmly conclude that the EL around 480−540 nm is due to the exciplex emission occurring at the interface of NPB and **AlmND$_3$**. It is rather common that electron-deficient materials (such as **Alq$_3$** and 1,3,4-oxadiazole compounds) have a propensity to form exciplex with electron-rich hole-transporting materials (such as NPB triarylamine species).[19] By lowering the HOMO energy level of the hole-transporting material (i.e., reducing the HOMO energy level difference between the hole-transporting material and **AlmND$_3$**),[19d] the problem of the exciplex associated with **AlmND$_3$** can be largely alleviated. As shown in Figure 7, having a low HOMO energy level around 6.1 eV,[20] arylamine *m*CP (1,3-di(9*H*-carbazol-9-yl)benzene) is effective in preventing the exciplex emission as evident in device ITO/NPB(30 nm)/mCP(30 nm)/**AlmND$_3$**(30 nm)/LiF(5 nm)/Al (150 nm), although such a device is very poor in EL efficiency and brightness. Also having a low HOMO energy level around 6.3 eV,[21] another hole-transporting material CBP (4,4′-di(9*H*-carbazol-9-yl)biphenyl) was thus inserted between NPB and **AlmND$_3$**. By the variation of CBP layer thickness, we have successfully eliminated the exciplex emission and optimize the performance of the blue devices ITO/NPB(40 nm)/CBP(x nm)/**AlmND$_3$**(30 nm)/**Alq$_3$** (20 nm)/LiF (5 nm)/Al (150 nm) optimized with $x = 10$ (Table 2). From such CBP-inserted nondoped **AlmND$_3$** OLEDs, we have successfully achieved deep blue ELs ($CIE_{x,y} = 0.15$, 0.10) with a reasonably good external quantum efficiency (η_{ext}) reaching 1.79% (or 1.63% at 20 mA/cm^2) and a maximum brightness of 5070 cd/m^2 (or 277 cd m^{-2} at 20 mA/cm^2) (Figure 8). To the best of our knowledge, we believe that a similar exciplex problem of **AlmND$_3$** has been found for **AlND$_3$** before and the problem has not been solved until this study.[22]

Table 2. Electroluminescence Characteristics of Nondoped **AlmND$_3$** OLEDs Containing CBP with Different Layer Thickness[a]

CBP thickness [nm]	max. luminance, voltage [cd/m^2, V]	luminance, efficiency, voltage [cd/m^2, %, V][b]	max. efficiency [%, cd/A, lm/W]	λ_{max}^{el} [nm]	CIE 1931 chromaticity [x, y]
3	5555, 15	119, 0.39, 5.68	0.53, 0.79, 0.33	456	0.18, 0.20
5	4971, 15	162, 0.86, 5.63	1.08, 1.01, 0.45	450	0.15, 0.11
10	5070, 15	277, 1.63, 8.37	1.79, 1.51, 0.53	448	0.15, 0.10
15	5606, 15	315, 1.63, 9.55	1.74, 1.68, 0.53	452	0.16, 0.12

[a] Devices have the configuration of ITO/NPB(40 nm)/CBP(x nm)/**AlmND$_3$**(30 nm)/**Alq$_3$**(20 nm)/LiF(0.5 nm)/Al(150 nm), x = 3, 5, 10, and 15, respectively. [b] At current density of 20 mA/cm^2.

2.6. As Electron-Transporting Material in Non-Doped AlmND$_3$ OLEDs. Similar to green emitter **Alq$_3$**, deep blue emitter **AlmND$_3$** potentially can be used as an electron-transporting material in OLEDs. To gauge such viability, four nondoped **AlmND$_3$** OLEDs containing four different ETL materials were fabricated: ITO/NPB(40 nm)/CBP10 nm)/**AlmND$_3$**(30 nm)/ETL(20 nm)/LiF(5 nm)/Al(150 nm), where the ETL material is TPBI (2,2′,2″-(1,3,5-phenylene)tris(1-phenyl-1*H*-benzimidazole), Bebq$_2$ (beryllium bis(benzoquinolin-10-olate), **Alq$_3$**, or **AlmND$_3$**. As data have shown in Table 3 and Figure 9, in terms of η_{ext}, nondoped **AlmND$_3$** OLEDs are most efficient when **AlmND$_3$** is employed as the ETL material in OLEDs, although it is not as bright as others. However, in terms of power efficiency (η_P), nondoped **AlmND$_3$** OLEDs having TPBI or Bebq$_2$ are more efficient than ones using **Alq$_3$** or **AlmND$_3$** as the ETL materials (Table 3). We notice that **AlmND$_3$** provide OLEDs a relatively low current density and a relatively high turn-on voltage (Figure 9), which are comparable with those of **Alq$_3$** but inferor to those of TPBI or Bebq$_2$. Nevertheless, such results validate the usage of **AlmND$_3$** as an ETL material in OLEDs.

2.7. AlND$_3$, AlmND$_3$, AlmmND$_3$, and AlmpND$_3$ for High Efficiency Non-Doped Deep Blue OLEDs. Having solved the problem of exciplex EL and demonstrated the electron-

(19) (a) Itano, K.; Ogawa, H.; Shirota, Y. *Appl. Phys. Lett.* **1998**, *72*, 636. (b) Chan, L.-H.; Lee, R.-H.; Hsieh, C.-F.; Yeh, H.-C.; Chen, C.-T. *J. Am. Chem. Soc.* **2002**, *124*, 6469. (c) Guan, M.; Bian, Z. Q.; Zhou, Y. F.; Li, F. Y.; Li, Z. J.; Huang, C. H. *Chem. Commun.* **2003**, 2708. (d) Matsumoto, N.; Nishiyama, M.; Adachi, C. *J. Phys. Chem. C* **2008**, *112*, 7735.

(20) Wu, M.-F.; Yeh, S.-J.; Chen, C.-T.; Murayama, H.; Tsuboi, T.; Li, W.-S.; Chao, I.; Liu, S.-W.; Wang, J.-K. *Adv. Funct. Mater* **2007**, *17*, 1887.

(21) Hill, I. G.; Rajagopai, A.; Kahn, A. *J. Appl. Phys.* **1998**, *84*, 3236.

(22) Chen, Chin Hsin, Department of Photonics and Display Institute, National Chiao Tung University, private communication.

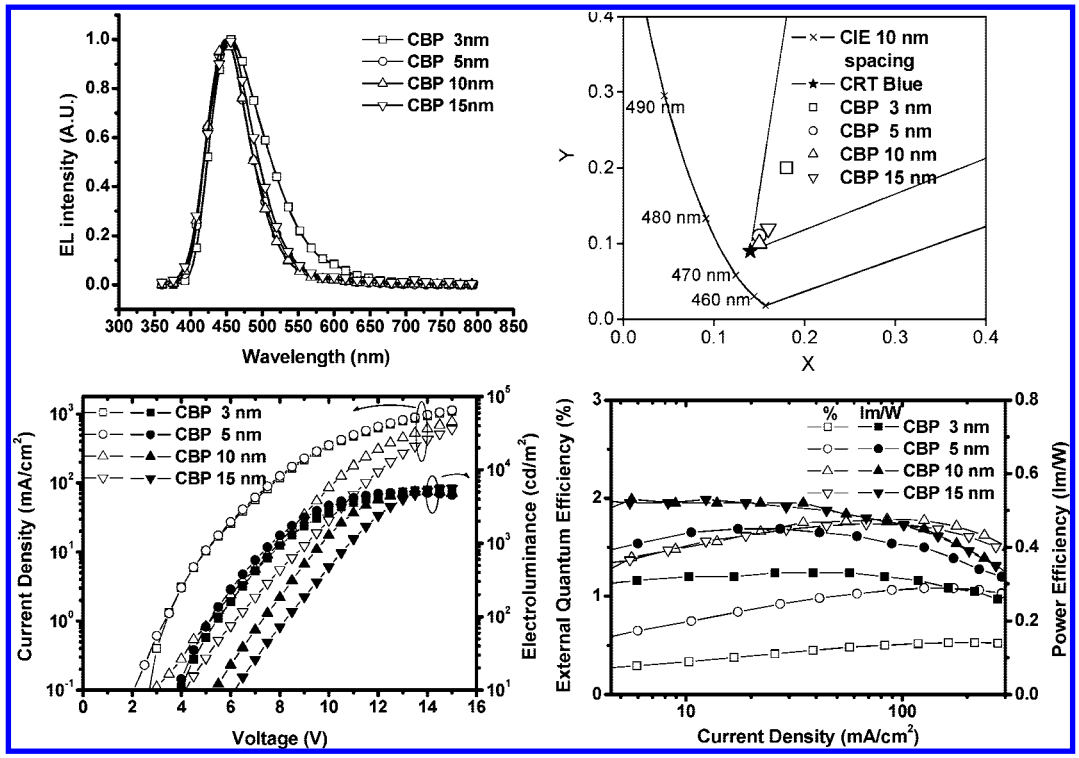

Figure 8. EL characteristics of ITO/NPB(40 nm)/CBP(x nm)/**AlmND$_3$**(30 nm)/**Alq$_3$**(20 nm)/LiF(0.5 nm)/Al(150 nm), x = 3, 5, 10, and 15, respectively.

Table 3. Electroluminescence Characteristics of Nondoped **AlmND$_3$** OLEDs with Various ETL Materials[a]

ETL	max. luminance and voltage [cd/m^2, V]	luminance, efficiency, voltage [cd/m^2, %, V][b]	max. efficiency [%, cd/A, lm/W]	λ_{max}^{el} [nm]	CIE 1931 chromaticity [x, y]
TPBI	6000, 15	240, 1.15, 6.2	1.86, 1.79, 0.86	454	0.16, 0.13
Bebq$_2$	7140, 15	340, 1.67, 5.6	1.81, 1.84, 0.98	458	0.15, 0.13
Alq$_3$	5070, 15	277, 1.63, 8.4	1.79, 1.51, 0.53	448	0.15, 0.10
AlmND$_3$	5240, 15	310, 1.85, 6.8	1.96, 1.65, 0.84	452	0.15, 0.10

[a] ITO/NPB(40 nm)/CBP(10 nm)/**AlmND$_3$**(30 nm)/ETL(20 nm)/LiF(5 nm)/Al(150 nm). [b] At 20 mA/cm^2.

transporting property of **AlmND$_3$**, we are ready to examine and find the best aluminum chelates of **ND**, **mND**, **mmND**, and **mpND** for nondoped deep blue OLEDs. Having **AlmND$_3$** as the electron-transporting layer, four nondoped OLEDs were based on **AlND$_3$**, **AlmND$_3$**, **AlmmND$_3$**, and **AlmpND$_3$**: ITO/NPB(40 nm)/CBP(10 nm)/Blue Al chelates(30 nm)/**AlmND$_3$**(20 nm)/LiF(0.5 nm)/Al(150 nm) were fabricated and characterized (Table 4 and Figure 10).

As it can be anticipated from their solution or solid-state fluorescence wavelength, the **AlmND$_3$** OLED showed a much deeper blue EL with 1931 Commision Internationale de L'Eclairage x, y coordinates (CIE$_{x,y}$ = 0.15, 0.09) than that of **AlND$_3$** OLED (CIE$_{x,y}$ = 0.15, 0.19). However, we do not anticipate that **AlmND$_3$** OLED performs better than does **AlND$_3$** OLED considering its fluorescence quantum yield. Since fluorescence quantum yields of **AlND$_3$** are higher than those of **AlmND$_3$** either in solution or in the solid state, we attribute such a result to the charge balancing in the OLED, which has a great influence on the efficiency of the charge-recombination in the OLED. More surprisingly, the **AlmmND$_3$** OLED shows the shortest EL wavelength (λ_{max}^{EL} ~436 nm), the highest η_{ext} of 4.18% (or 4.11% at 20 mA/cm^2), and the brightest EL of 445 cd/m^2 at 20 mA/cm^2. Considering the structural difference among **AlND$_3$**, **AlmND$_3$**, and **AlmmND$_3$**, it is hard to conceive that an insignificant methyl substituent or the number of methyl substituents can exert that much on η_{ext} and EL brightness. Plausibly, among four aluminum chelates, we may recognize **AlmmND$_3$** as an exceptional one based on the red-shifted fluorescence from solution to the solid state. The red-shifting fluorescence is 443→447 nm, 415→431 nm, 416→419 nm, and 417→425 nm for **AlND$_3$**, **AlmND$_3$**, **AlmmND$_3$**, and **AlmpND$_3$**, respectively. Energywise, this corresponds to a red-shifting energy of 723, 895, 172, and 451 cm^{-1}, respectively for four aluminum chelates. **AlmmND$_3$** has the smallest red-shifted fluorescence among all. Accordingly, we surmise that, in the solid state, **AlmmND$_3$** aggregates in a quite different fashion from the other aluminum chelates. Compared with other aluminum chelates, such aggregation enables high efficiency of charge recombination (or charge balance) and thus the η_{ext} (or η_P) of **AlmmND$_3$** OLEDs. For **AlmmND$_3$**, the low hole mobility (lower than its electron mobility) helps in balancing the charge of **AlmmND$_3$** OLEDs.

We have also examined the performance of blue OLEDs with **GamND$_3$**, **GammND$_3$**, **InmND$_3$**, or **InmmND$_3$** as the nondoped light-emitting layer (Table S1). As it can be anticipated from the fact that a heavy atom will quench the fluorescence, indium chelates performed the worst in terms of EL efficiency or brightness. However, this is not exactly the case for gallium chelates. Comparing data in Table 4 and Table S1, the **GammND$_3$** OLED is worse than the **AlmmND$_3$** OLED but the **GamND$_3$** OLED is better than the **AlmND$_3$** OLED. Nevertheless, once again, we verified the same trend of OLED performance; namely, **mmND** is better than **mND** for gallium or indium metal chelates as nondoped deep blue light-emitting materials for OLEDs.

2.8. Nondoped AlmmND$_3$ OLEDs with Various Metal Chelates as Electron-Transporting Layer. Knowing all group III metal chelates are potential ETL material in OLEDs, we fabricated a series of **AlmmND$_3$**-based nondoped blue OLEDs

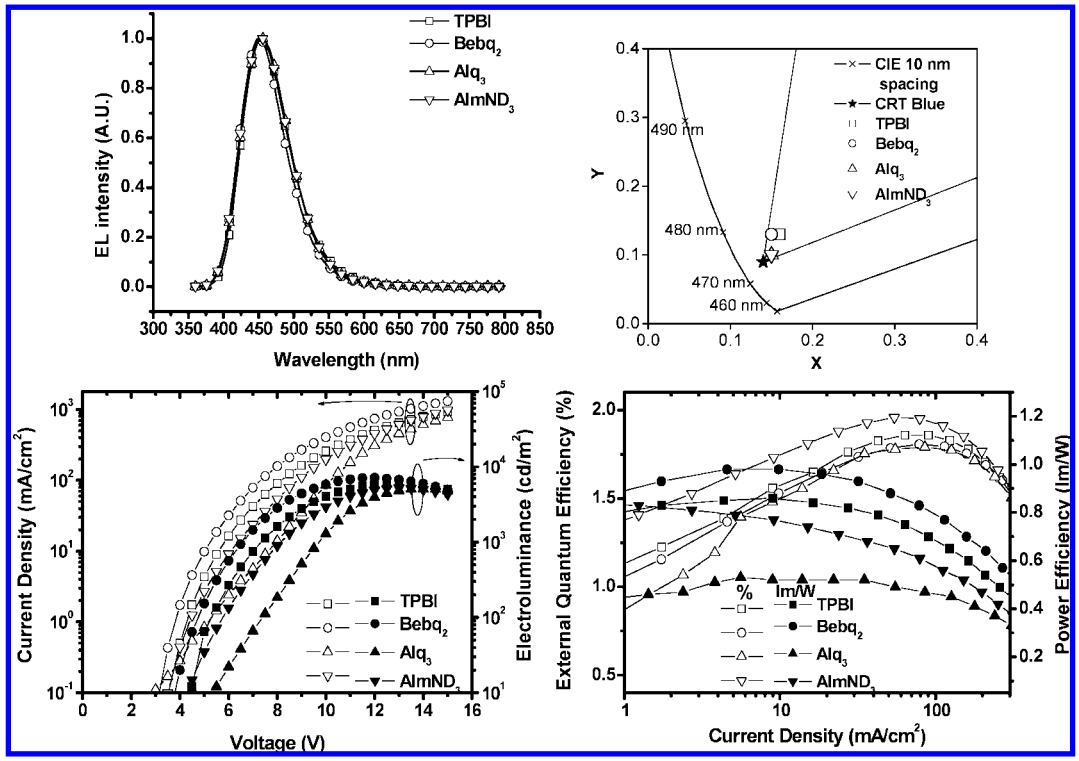

Figure 9. EL characteristics of ITO/NPB(40 nm)/CBP(10 nm)/**AlmND$_3$**(30 nm)/ETL(20 nm)/LiF(0.5 nm)/Al(150 nm), where ETL is TPBI, Bebq$_2$, **Alq$_3$**, and **AlmND$_3$**, respectively.

Table 4. Electroluminescence Characteristics of Nondoped OLEDs of **AlND$_3$**, **AlmND$_3$**, **AlmmND$_3$**, and **AlmpND$_3$** blue Al chelates[a]

Al chelates	max. luminance and voltage [cd/m^2, V]	luminance, efficiency, voltage [cd/m^2, %, V] [b]	max. efficiency [%, cd/A, lm/W]	λ_{max}^{el} [nm]	CIE 1931 chromaticity [x, y]
AlND$_3$	2286, 15	216, 0.75, 8.31	0.76, 1.09, 0.45	466	0.15, 0.19
AlmND$_3$	3824, 15	279, 1.86, 7.57	1.91, 1.43, 0.77	448	0.15, 0.09
AlmmND$_3$	3792, 15	445, 4.11, 9.36	4.18, 2.27, 0.86	436	0.15, 0.07
AlmpND$_3$	4078, 15	306, 1.58, 9.63	1.62, 1.58, 0.71	452	0.15, 0.12

[a] Devices have the configuration of ITO/NPB(40 nm)/CBP(10 nm)/Blue Al chelates(30 nm)/**AlmND$_3$**(20 nm)/LiF(0.5 nm)/Al(150 nm). [b] At current density of 20 mA/cm^2.

with a variation of ETL material, **AlND$_3$**, **AlmND$_3$**, **AlmmND$_3$**, **AlmpND$_3$**, **GamND$_3$**, or **InmND$_3$** (Table 5 and Figure S2). Here, for a fair comparison, the **AlmmND$_3$** OLED having **AlmND$_3$** as ETL material is a refabricated one, not the same one in Table 4 and Figure 10. As the data show in Table 5, all devices exhibit virtually the same λ_{max}^{el} 432 nm and a very similar deep blue color chromaticity CIE$_{x,y}$ = 0.15−0.16, 0.07−0.08, consistent with all OLEDs having the same deep blue nondoped emitter **AlmmND$_3$**. Regardless of ETL materials, all deep blue OLEDs have a relatively high EL efficiency with η_{ext} being more than 3.0%. In terms of EL efficiency, the **AlmmND$_3$** OLED having **AlmND$_3$** as the ETL material is the most outstanding. This OLED has η_{ext} reaching 3.77% and η_P over 0.80 lm/W at a current density of 20 mA/cm^2. From OLED results in section 2.7 and 2.8, it is very clear that **AlmmND$_3$** is the most efficient nondoped deep blue emitter but **AlmND$_3$** is the best ETL material for it.

2.9. AlmND$_3$ as the Host Material for Blue Perylene and Deep Blue 9,10-Diphenylanthracene Dopants. To demonstrate the wide band gap nature of hydroxynaphthyridine metal chelates, we have fabricated a series of **AlmND$_3$** OLEDs containing perylene or 9,10-diphenylanthracene (DPA) as highly efficient blue or deep blue dopant materials. Perylene is a highly fluorescent blue emitter with λ_{max}^{fl} 467 nm (in clyclohexane) and Φ_f 94%.[23] However, in the solid state blue perylene becomes a poor fluorophore, a yellow one, due to the severe molecular aggregation that brings about concentration quenching, and a diminished and red-shifting fluorescence takes place. The fluorescence of DPA is even bluer and stronger showing λ_{max}^{fl} 438 nm (in cyclohexane) and Φ_f 100%.[23] Similar to blue perylene, deep blue DPA has the inherent problem of crystallizing when deposited as a thin film that prohibits its nondopant usage in a device.[24] Whereas some reports are available for the dopant usage of perylene,[25] there is no known literature case of the dopant usage of DPA in OLEDs to date. This can be simply attributed to the lack of appropriate host material, a wide band gap one, required for such a deep blue DPA dopant.

We took 0.5, 2, and 4 wt % dopant concentration of both perylene and DPA in the fabrication of dopant-based **AlmND$_3$** OLEDs. The EL characteristics of both series of devices are displayed in Figures 11 and 12, and their data are summarized in Table 6.

(23) Berlman, I. B. *Handbook of Fluorescence Spectra of Aromatic Molecules*, 2nd ed.; Academic Press: New York, 1971; pp 264 and 399.
(24) Adachi, C.; Tsutsui, T.; Sato, S. *Appl. Phys. Lett.* **1990**, *56*, 799.
(25) (a) Kojima, H.; Ozawa, A.; Takahshi, T.; Nagaoka, M.; Homma, T.; Nagatomo, T.; Omoto, O. *J. Electrochem. Soc.* **1997**, *144*, 3628. (b) Mi, B. X.; Gao, Z. Q.; Lee, C. S.; Lee, C. T.; Kwong, H. L.; Wong, N. B. *App. Phys. Lett.* **1999**, *75*, 4055. (c) Lu, P.; Hong, H.; Cai, G.; Djurovich, P.; Weber, W. P.; Thompson, M. E. *J. Am. Chem. Soc.* **2000**, *122*, 7480. (d) Jiang, X.-Y.; Zhang, Z.-L.; Zheng, Z.-Y.; Wu, Y.-Z.; Xu, S.-H. *Thin Solid Films* **2001**, *401*, 251. (e) Wu, C.-C.; Lin, Y.-T.; Chiang, H.-H.; Cho, T.-Y.; Chen, C.-W.; Wong, K.-T.; Liao, Y.-L.; Lee, G.-H.; Peng, S.-M. *Appl. Phys. Lett.* **2002**, *81*, 577. (f) Ni, S. Y.; Wang, X. R.; Wu, Y. Z.; Chen, H. Y.; Zhu, W. Q.; Jiang, X. Y.; Zhang, Z. L.; Sun, R. G. *Appl. Phys. Lett.* **2004**, *85*, 878. (g) Jarikov, V. V. *J. Appl. Phys.* **2006**, *100*, 014901. (h) Tse, S.-C.; Tsung, K.-K.; So, S.-K. *Appl. Phys. Lett.* **2007**, *90*, 213502. (i) Lee, R.-H.; Hung, Y.-W.; Wang, Y.-Y.; Chang, H.-Y. *Thin Solid Films* **2008**, *516*, 5062.

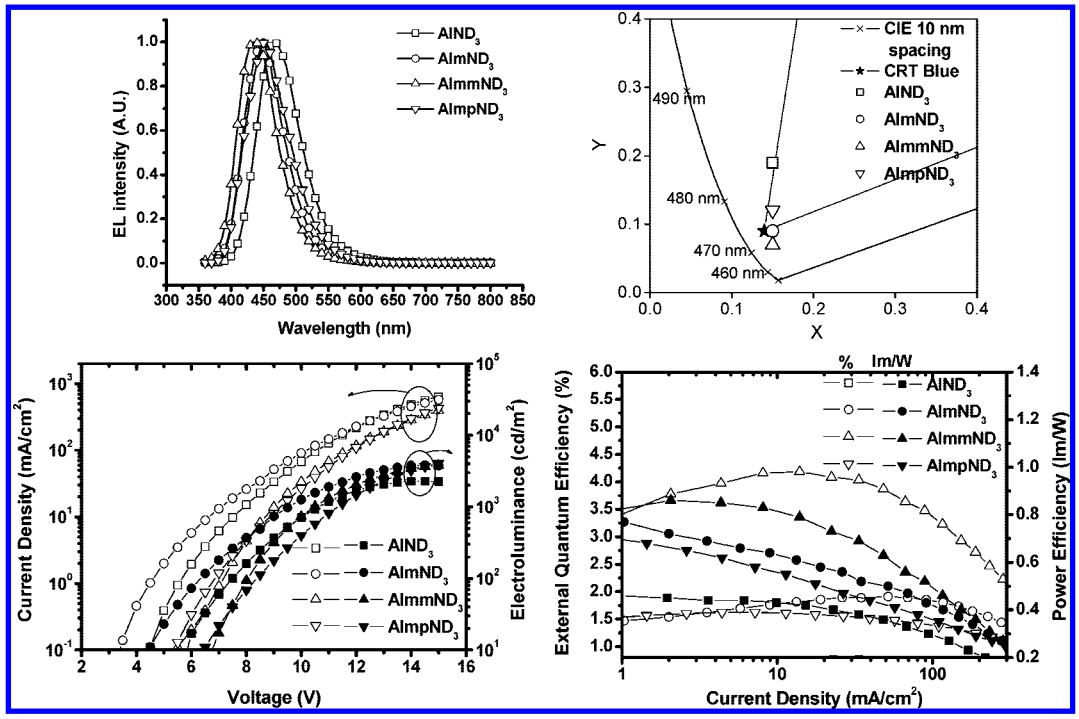

Figure 10. EL characteristics of ITO/NPB(40 nm)/CBP(10 nm)/Blue Al chelate(30 nm)/ETL(20 nm)/LiF(0.5 nm)/Al(150 nm), where Blue Al chelate is **AlND$_3$**, **AlmND$_3$**, **AlmmND$_3$**, and **AlmpND$_3$**, respectively.

Table 5. Electroluminescence Characteristics of Nondoped OLEDs of **AlmmND$_3$** with Various Metal Chelates as ETL Materials[a]

ETL	max. luminance and voltage [cd/m^2, V]	luminance, efficiency, voltage [cd/m^2, %, V] [b]	max. efficiency [%, cd/A, lm/W]	λ_{max}^{el} [nm]	CIE 1931 chromaticity [x, y]
AlND$_3$	3313, 15	369, 3.40, 8.92	3.67, 2.00, 1.04	432	0.15, 0.07
AlmND$_3$	4444, 15	401, 3.77, 7.75	3.79, 2.00, 0.94	432	0.15, 0.07
AlmmND$_3$	4879, 15	329, 3.01, 8.60	3.27, 1.78, 0.84	432	0.16, 0.07
AlmpND$_3$	5487, 15	376, 3.23, 8.24	3.41, 1.99, 1.13	432	0.16, 0.08
GamND$_3$	4694, 15	416, 3.67, 8.18	3.68, 2.09, 0.93	432	0.15, 0.07
InmND$_3$	3848, 15	376, 3.62, 8.62	3.67, 1.91, 0.91	432	0.15, 0.07

[a] Devices have the configuration of ITO/NPB(40 nm)/CBP(10 nm)/**AlmmND$_3$**(30 nm)/ETL(20 nm)/LiF(0.5 nm)/Al(150 nm). [b] At current density of 20 mA/cm^2.

Dopant concentration 0.5 wt% was found to be optimum for either perylene or DPA. The vibronic emission observed at the low energy side of the major EL band is the distinct feature of a not so blue preylene EL, indicating a sufficient Förster energy transfer between the **AlmND$_3$** host and perylene dopant. Compared to the undoped device (second entry of Table 4), the maximum EL efficiency of the perylene-doped device was enhanced more than four times to ~3.06 lm/W, or more than three times to ~4.67 cd/A. At a current density of 20 mA/cm^2, η_{ext} was 3.13%, which was enhanced 1.7 times compared to an undoped device. The maximum electroluminance also increased to 12 420 cd/m^2, a greater than 3-fold enhancement than that of the undoped device, although this is at a price of deep blue color purity. The perylene-doped device had a chromaticity of CIE$_{x,y}$ = 0.14, 0.17, less deep blue than CIE$_{x,y}$ = 0.15, 0.09 of the undoped device (second entry of Table 4). Nonetheless, the performance of the 0.5 wt% perylene-doped **AlmND$_3$** OLED reported herein is one of the best perylene dopant devices known in literature.[25] Similar enhancement of the OLED performance was also observed for DPA-doped devices, although the enhancement was to a smaller extent when compared with that of perylene-doped OLEDs. However, the deep blue color purity was elevated to a higher level, CIE$_{x,y}$ = 0.15, 0.06. After the comparison with emission spectra of solution DPA, solid state **AlmND$_3$**, and solid state DPA (fluorescence spectra shown in Figure 12), the EL spectra of the DPA-doped **AlmND$_3$** OLED can be recognized as a coemission from both DPA and **AlmND$_3$**. Since the main emission wavelength of DPA is shorter than that for **AlmND$_3$**, the coemission EL observed for the DPA-doped **AlmND$_3$** OLED gave rise to the deepest blue color (see inserted 1931 CIE chromaticity diagram in Figure 12). Considering the inadequate overlapping of the absorption spectrum of DAP and the emission spectrum of **AlmND$_3$** (not shown in Figure 12), we can conceive that Förster energy transfer between

(26) (a) Xie, Z. Y.; Huang, J. S.; Li, C. N.; Liu, S. Y.; Wang, Y.; Li, Y. Q.; Shen, J. C. *Appl. Phys. Lett.* **1999**, *74*, 641. (b) Steuber, F.; Staudigel, J.; Strössel, M.; Simmerer, J.; Winnacker, A.; Spreitzer, H.; Weissörtel, F.; Salbeck, J. *Adv. Mater.* **2000**, *12*, 130. (c) Xie, Z. Y.; Feng, J.; Huang, J. S.; Liu, S. Y.; Wang, Y.; Shen, J. C. *Synth. Met.* **2000**, *108*, 81. (d) Zhang, Z.; Jiang, X.; Xu, S. *Thin Solid Films* **2000**, *363*, 61. (e) Liu, S.; Hunag, J.; Xie, Z.; Wang, Y.; Chen, B. *Thin Solid Films* **2000**, *363*, 294. (f) Chuen, C. H.; Tao, Y. T. *Appl. Phys. Lett.* **2002**, *81*, 4499. (g) Li, G.; Shinar, J. *Appl. Phys. Lett.* **2003**, *83*, 5359. (h) Cheng, G.; Zhao, Y.; Zhang, Y.; Liu, S.; He, F.; Zhang, H.; Ma, Y. *Appl. Phys. Lett.* **2004**, *84*, 4457. (i) Liu, T.-H.; Wu, Y.-S.; Lee, M.-T.; Chen, H.-H.; Liao, C.-H.; Chen, C. H. *Appl. Phys. Lett.* **2004**, *85*, 4304. (j) Cheng, G.; Xie, Z.; Zhao, Y.; Zhang, Y.; Xia, H.; Ma, Y.; Liu, S. *Thin Solid Films* **2005**, *484*, 54. (k) Xie, W.; Meng, M.; Li, C.; Zhao, Y.; Liu, S. *Opt. Quant. Electron.* **2005**, *37*, 943. (l) Li, M.; Li, W.; Niu, J.; Chu, B.; Li, B.; Sun, X.; Zhang, Z.; Hu, Z. *Solid-State Electron.* **2005**, *49*, 1956. (m) Tao, S.; Peng, Z.; Zhang, X.; Wu, S. *J. Lumin.* **2006**, *121*, 568. (n) Zhang, G. H.; Hua, Y. L.; Petty, M. C.; Wu, K. W.; Zhu, F. J.; Niu, X.; Hui, J. L.; Liu, S.; Wu, X. M.; Yin, S. G.; Deng, J. C. *Displays* **2006**, *27*, 187. (o) Choukri, H.; Fischer, A.; Forget, S.; Chénais, S.; Castex, M.-C.; Adés, D.; Slove, A.; Geffroy, B. *Appl. Phys. Lett.* **2006**, *89*, 183513. (p) Hsiao, C.-H.; Lin, C.-F.; Lee, J.-H. *J. Appl. Phys.* **2007**, *102*, 094508. (q) Huang, H.-H.; Chu, S.-Y.; Kao, P.-C.; Chen, Y.-C. *Thin Solid Films* **2008**, *516*, 5669. (r) Tang, S.; Liu, M.; Lu, P.; Cheng, G.; Zeng, M.; Xie, Z.; Xu, H.; Wang, H.; Yang, B.; Ma, Y.; Yan, D. *Org. Electron.* **2008**, *9*, 241. (s) Duan, Y.; Mazzeo, M.; Maiorano, V.; Mariano, F.; Qin, D.; Cingolani, R.; Gigli, G. *Appl. Phys. Lett.* **2008**, *92*, 113304.

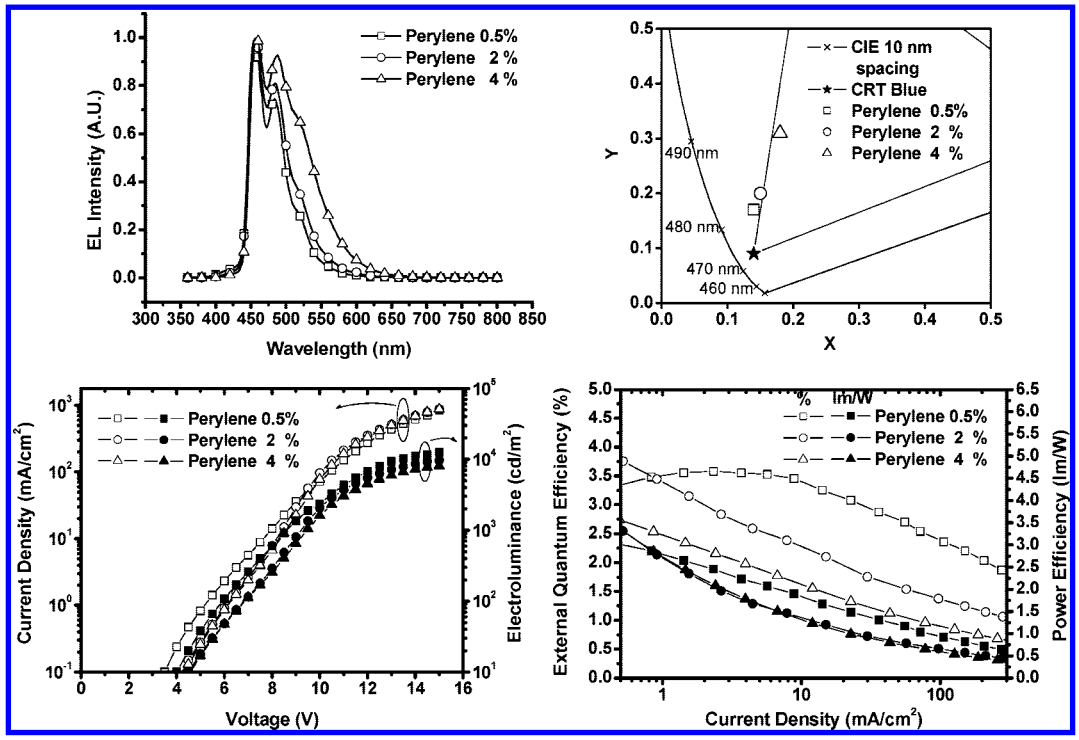

Figure 11. EL characteristics of ITO/NPB(40 nm)/CBP(10 nm)/**AlmND$_3$**:perylene(*x* %, 30 nm)/**AlmND$_3$**(20 nm)/LiF(0.5 nm)/Al(150 nm), where *x* is 0.5, 2, or 4, the weight percent of perylene dopant.

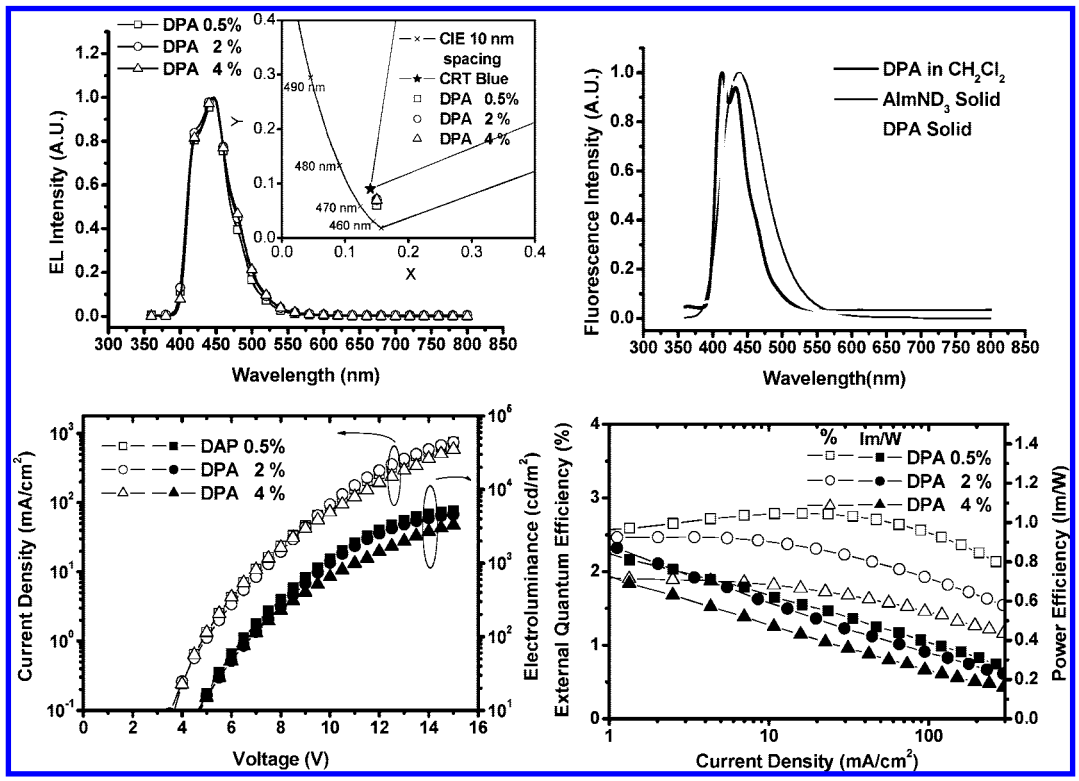

Figure 12. EL characteristics of ITO/NPB(40 nm)/CBP(10 nm)/**AlmND$_3$**:DPA(*x* %, 30 nm)/**AlmND$_3$**(20 nm)/LiF(0.5 nm)/Al(150 nm), where *x* is 0.5, 2, or 4, the weight percent of DPA dopant

the **AlmND$_3$** host and DPA dopant is somewhat incomplete, even though the HOMO energy level of the **AlmND$_3$** host is low enough for the DPA dopant (but the LUMO energy level of **AlmND$_3$** is not high enough for the DPA dopant). Despite such a coemission, to the best of our knowledge, this is the first observation of a deep blue EL from DPA.

2.10. AlmND$_3$ as the Host Material for High Efficiency White OLEDs with Rubrene Yellow Dopant. Yellow fluorophore rubrene is probably the most commonly used dopant accompanying blue fluorescent host material in the fabrication of white OLEDs.[26,27] Fluorescence spectrum of **AlmND$_3$** is partially overlapping with the absorption spectrum of rubrene

Table 6. Electroluminescence Characteristics of **AlmND$_3$** OLEDs with Various Dopant (Perylene or 9,10-Diphenylanthracene) Concentrations[a]

dopant concn [wt %]	max. luminance and voltage [cd/m^2, V]	luminance, efficiency, voltage [cd/m^2, %, V][b]	max. efficiency [%, cd/A, lm/W]	λ_{max}^{el} [nm]	CIE 1931 chromaticity [x, y]
Perylene as Dopant					
0.5	12420, 15	810, 3.13, 8.3	3.56, 4.67, 3.06	456	0.14, 0.17
2	9610, 15	590, 1.98, 8.7	3.77, 3.51, 3.28	456	0.15, 0.20
4	8060, 15	580, 1.38, 8.9	2.73, 5.45, 3.69	458	0.18, 0.31
9,10-Diphenylanthracene (DPA) as Dopant					
0.5	5120, 15	278, 2.78, 5.8	2.80, 1.39, 0.89	448	0.15, 0.06
2	4595, 15	259, 2.31, 5.4	2.47, 1.38, 0.87	446	0.15, 0.07
4	3295, 15	203, 1.75, 5.6	1.90, 1.91, 0.69	446	0.18, 0.07

[a] ITO/NPB(40 nm)/CBP(10 nm)/**AlmND$_3$**:Dopant (x %, 30 nm)/**AlmND$_3$**(20 nm)/LiF(5 nm)/Al(150 nm), where x = 0.5, 2, and 4 (weight percent) for perylene or 9,10-diphenylanthracene (DPA) dopant. [b] At 20 mA/cm^2.

(Figure S3 left), and white fluorescence is feasible with an appropriate ratio of mixed **AlmND$_3$** and rubrene (Figure S3 right).

We have demonstrated that the deep blue **AlmND$_3$** is a good host material for rubrene in generating high EL efficiency white OLEDs. A series of OLEDs ITO/NPB(40 nm)/CBP(10 nm)/**AlmND$_3$**:rubrene(x %, 30 nm)/**AlmND$_3$**(20 nm)/LiF(0.5 nm)/Al(150 nm) with a variation of rubrene dopant concentration 0.5−4 wt% and EL characteristics of such **AlmND$_3$**:rubrene OLEDs are shown in Figure 13 and their data are summarized in Table 7.

Similar to most rubrene-based white OLEDs, an authentic white color purity (CIE$_{x,\,y}$ = 0.32, 0.38) was achieved at a very low dopant concentration, 0.5 wt % of **AlmND$_3$** (first entry of Table 7). Any higher dopant concentration simply impairs the white color purity of OLEDs. For such white OLEDs at a brightness of 100 cd/m^2, η_{ext} is 4.25%, which is equivalent to an η_P of 8.67 lm/W, one of the highest among literature-known rubrene-based white OLEDs.[26,27] The color rendering index (CRI) of such white (two-color-component) OLEDs was determined to be in the range 45−50, and it is in general inferior to CRI ∼80 of three-color-component white OLEDs.[28] At practical lighting conditions, i.e., 1000 cd/m^2, such an **AlmND$_3$**:rubrene white OLED has an η_{ext} of ∼3.9% or η_P of 5.1 lm/W (Figure 13). With few exceptions,[27] this EL efficiency at 1000 cd/m^2 also outperforms most literature-known rubrene-based two-element white OLEDs. Also, a doped device with a 4% rubrene concentration is virtually a yellow OLED, CIE$_{x,\,y}$ = 0.45, 0.51 (Figure 13 and the fourth entry of Table 7). Its high efficiency, 4.56%, 15.83 cd/A, or 11.94 lm/W, at 100 cd/m^2 and high brightness (1930 cd/m^2 at 20 mA/cm^2) outperforms most currently known yellow OLEDs.[29] The high EL efficiency of such rubrene-based white or yellow OLEDs can be attributed to the high electron mobility of **AlmND$_3$**. High electron mobility is rarely observed for the host material in the white or yellow OLEDs, and it facilitates the charge balance and hence the EL efficiency of OLEDs.

3. Conclusion

We have reported the first series of group III metal chelates as the authentic deep blue analogues of green **Alq$_3$**. A large quantity of these deep blue metal chelates are readily available now due to our improved synthesis and facial purification method applicable for them. Unlike several currently known blue analogues of **Alq$_3$**, these deep blue group III metal chelates are volatile and thermally stable enough for OLED fabrication by a vacuum-thermal-deposition process. For OLEDs, we have overcome the problem of exciplex formation, which has hampered **AlND$_3$** from practical usage in OLEDs before. High efficiency (maximum η_{ext} > 4.0%) and deep blue (CIE$_{x,y}$ = 0.15, 0.07) nondoped OLEDs were achieved for **AlmmND$_3$**. The wide band gap of these deep blue metal chelates, 6.4 and 3.0 eV for **AlmND$_3$** HOMO and LUMO energy levels, respectively, enable their usage as the host material for perylene blue dopant or deep blue 9,10-diphenylanthracene. These group III metal chelates, particularly **AlmND$_3$** and **AlmmND$_3$**, have been characterized for the charge carrier mobility by a time-of-flight technique. Both **AlmND$_3$** and **AlmmND$_3$** exhibit high electron mobility, comparable with or even higher than that of BeBq$_2$ or **Alq$_3$**. Moreover, **AlmND$_3$** is ambipolar with a similar mobility of 10^{-4} cm^2/Vs for both hole and electron. The success of highly efficient white OLEDs (or yellow OLEDs) based on a rubrene dopant is attributed to the high electron (and hole) mobility of the host material, **AlmND$_3$**. We have demonstrated the versatile and effective application of hydroxynaphthyridine-based group III metal chelates for OLEDs. More high performance OLEDs can be anticipated now due to the availability of long-thought, wide band gap, deep blue group III metal chelates.

4. Experimental Section

General Information. Both solution and solid-state fluorescence quantum yields (Φ_f's) of the blue metal chelates were determined by the integrating-sphere method.[30] Photoluminescence (PL) spectra were recorded on a Hitachi fluorescence spectrophotometer F-4500, and the same spectrophotometer was used to record the EL spectra of OLEDs. Melting points (T_ms), glass transition temperatures (T_g's), and crystallization temperatures (T_c's) of respective compounds were measured via differential scanning calorimetry (DSC) using a Perkin-Elmer DSC-6 differential scanning calorimeter. The HOMO energy levels of the thin-film samples of metal chelates were studied by ultraviolet photoemission spectroscopy (UPS). The experimental detail of UPS measurement has been described before.[31] LUMO energy levels were estimated by subtracting the energy gap (ΔE) from HOMO energy levels. ΔE was determined by the on-set absorption energy from the absorption spectra of the materials. UV−visible electronic absorption spectra were recorded on a Hewlett-Packard 8453 Diode Array spectrophotometer. The method of time-of-flight (TOF) in measuring charge carrier mobility has been reported before.[32] Data collection of the X-ray crystallography analysis was carried out on a Brucker X8APEX CCD

(27) (a) Huang, J.; Li, G.; Wu, E.; Xu, Q.; Yang, Y. *Adv. Mater.* **2006**, *18*, 114. (b) Huang, J.; Hou, W.-J.; Li, J.-H.; Li, G.; Yang, Y. *Appl. Phys. Lett.* **2006**, *89*, 133509. (c) Tsai, Y.-C.; Jou, J.-H. *Appl. Phys. Lett.* **2006**, *89*, 243521.
(28) (a) D'Andrade, B. W.; Forrest, S. R. *Adv. Mater.* **2004**, *16*, 1585. (b) Misra, A.; Kumar, P.; Kamalasanan, Chandra, S. *Semicomd. Sci. Technol.* **2006**, *21*, R35. (c) Yeh, S.-J.; Chen, H.-Y.; Wu, M.-F.; Chan, L.-H.; Chiang, C.-L.; Yeh, H.-C.; Chen, Lee, J.-H. *Org. Electron.* **2006**, *7*, 137.
(29) See: Chiang, C.-L.; Tseng, S.-M.; Chen, C.-T.; Hsu, C.-P.; Shu, C.-F. *Adv. Funct. Mater* **2008**, *18*, 248, and references therein.
(30) (a) de Mello, J. C.; Wittmann, H. F.; Friend, R. H. *Adv. Mater.* **1997**, *9*, 230. (b) Chiang, C.-L.; Wu, M.-F.; Dai, D.-C.; Wen, Y.-S.; Wang, J.-K.; Chen, C.-T. *Adv. Funct. Mater* **2005**, *15*, 231.
(31) Wu, C.-I.; Lee, G.-R.; Lin, C.-T.; Chen, Y.-H.; Hong, Y.-H.; Liu, W.-G.; Wu, C.-C.; Wong, K.-T.; Chao, T.-C. *Appl. Phys. Lett.* **2005**, *87*, 242107.
(32) (a) Wu, M.-F.; Yeh, S.-J.; Chen, C.-T.; Murayama, H.; Tsuboi, T.; Li, W.-S.; Chao, I.; Liu, S.-W.; Wang, J.-K. *Adv. Funct. Mater.* **2007**, *17*, 1887. (b) Liu, S.-W.; Lee, J.-H.; Lee, C.-C.; Chen, C.-T.; Wang, J.-K. *Appl. Phys. Lett.* **2007**, *91*, 142106.

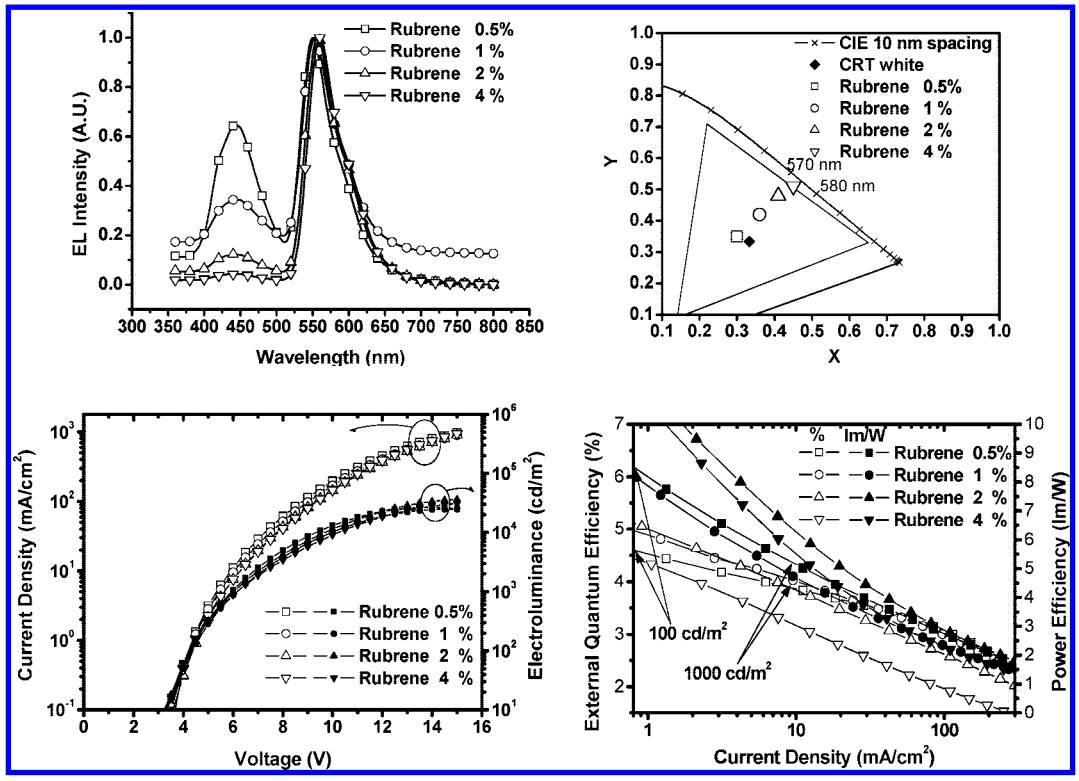

Figure 13. EL characteristics of ITO/NPB(40 nm)/CBP(10 nm)/**AlmND$_3$**:rubrene (*x* %, 30 nm)/**AlmND$_3$** (20 nm)/LiF(0.5 nm)/Al(150 nm), where *x* is 0.5, 1, 2, or 4, the weight percent of rubrene dopant. EL efficiency (η_{ext} or η_P) at 100 or 1000 cd/m^2 electroluminance is arrow-marked for the device with 0.5 wt% rubrene dopant.

Table 7. Electroluminescence Characteristics of White OLEDs with **AlmND$_3$** Host and Various Dopant (Rubrene) Concentration[a]

rubrene concn [wt %]	max. luminanceand voltage [cd/m^2, V]	luminance, efficiency, voltage [cd/m^2, %, V][b]	efficiency at 100 and 1000 cd/m^2 [%, cd/A, lm/W]	λ_{max}^{el} [nm]	CIE 1931 chromaticity [*x*, *y*]
0.5	26 710, 15	1830, 3.67, 6.58	4.25, 11.55, 8.67 3.91, 9.65, 5.13	444, 550	0.30, 0.35
1	24 810, 15	1670, 3.73, 6.75	4.97, 11.17, 8.20 3.97, 8.93, 4.58	444, 554	0.36, 0.42
2	36 290, 15	2260, 3.47, 7.02	5.35, 17.46, 13.03 3.98, 12.97, 6.78	444, 558	0.41, 0.48
4	30 970, 15	1930, 2.79, 7.05	4.56, 15.83, 11.94 3.24, 11.25, 5.77	444, 560	0.45, 0.51

[a] Devices have the configuration of ITO/NPB(40 nm)/CBP(10 nm)/**AlmND$_3$**:rubrene *x* %(30 nm)/AlmND(20 nm)/LiF(0.5 nm)/Al(150 nm), $x = 0.5$, 1, 2, 4, respectively. [b] At current density of 20 mA/cm.

diffractometer at 100 K for **AlND$_3$**·CH_2Cl_2 single crystals. The experimental detail of X-ray diffraction and their data process in solving the crystal structure can be found elsewhere.[30b]

The fabrication of OLEDs and their EL characterization also have been described before.[19b,33] The device was placed close to the photodiode such that all the forward light entered the photodiode. The effective size of the emitting diodes was 3.14 mm^2, which is significantly smaller than the active area of the photodiode dectector, a condition known as "under-fillling", satisfying the measurement protocol.[34] This is one of the most conventional ways in measuring the EL efficiency of OLEDs, although sometimes experimental errors may arise due to the non-Lambertian emission of OLEDs.[35] The color rendering index (CRI) of white OLEDs was measured by a spectroradiometer (Specbos 1201, JETI Technishe Instrumente GmbH).

(33) Yeh, S.-J.; Wu, M.-F.; Chen, C.-T.; Song, Y.-H.; Chi, Y.; Ho, M.-H.; Hsu, S.-F.; Chen, C. H. *Adv. Mater.* **2005**, *17*, 285.
(34) Forrest, S. R.; Bradley, D. D. C.; Thompson, M. E. *Adv. Mater.* **2003**, *15*, 1043.
(35) Tanaka, I.; Tokito, S. *Jpn. J. Appl. Phys* **2004**, *43*, 7733.

^{1}H and ^{13}C NMR specra were recorded on a Bruker AMX-400 MHz or AVA-400 MHz Fourier-transform spectrometer at room temperature. Elemental analyses (on a Perkin-Elmer 2400 CHN Elemental Analyzer) and electron impact (EI), fast atom bombardment (FAB), or matrix-assisted laser desorption/ionization time-of-flight (MALDI-TOF) mass spectra (on a VA Analytical 11-250J or 4800 MALDI TOF/TOF Analyzer) were recorded by the Elemental Analyses and Mass Spectroscopic Laboratory in-house service of the Institute of Chemistry, Academic Sinica.

Materials. For the materials used in device fabrication, Bebq$_2$, DPA (9,10-diphenylanthracene), perylene, and rubrene are commercially available materials and they were used without further purification. NPB (1,4-bis(1-naphthylphenylamino)biphenyl), CBP (4,4′-bis(9-carbazolyl)-2,2′-biphenyl), *m*CP (1,3-bis(9-carbazolyl)-benzene), TPBI (2,2′,2″-(1,3,5-phenylene)tris[1-phenyl-1*H*-benzimidazole]), and **Alq$_3$** were prepared via published methods and were subjected to gradient sublimation prior to use.

Synthesis of Tris(4-hydroxy-1,5-naphthyridinato)aluminum (AlND$_3$). To a toluene solution (4.5 mL) was added **ND** (0.15 g, 1.0 mmol) and aluminum triisopropoxide (0.07 g, 0.34 mmol). The

reaction mixture was heated at reflux under nitrogen for 1 h. During the reaction, a formation of milky white solid emitting blue fluorescence was observed. After cooling, the reaction solution was filtered to isolate a white solid. After washing with *n*-hexanes, the solid was subjected to zone-temperature sublimation. The pure product was isolated as a white solid. Yield: 76% (0.12 g). ^{1}H NMR (400 MHz, CD_2Cl_2): δ 8.77 (d, 1H, J = 4.75 Hz), 8.73−8.67 (m, 4H), 8.56 (d, 1H, J = 8.54 Hz), 8.51−8.47 (m, 2H), 7.73 (dd, 1H, J = 8.56 Hz, J = 4.72 Hz), 7.56 (dd, 1H, J = 8.60 Hz, J = 4.75 Hz), 7.49 (dd, 1H, J = 8.50 Hz, J = 4.74 Hz), 7.29 (d, 1H, J = 4.59 Hz), 6.93 (d, 1H, J = 5.33 Hz), 6.90 (d, 1H, J = 5.34 Hz), 6.81 (d, 1H, J = 5.32 Hz). ^{13}C NMR (100 MHz, $CDCl_3$): δ 165.17, 164.98, 164.65, 156.28, 155.73, 155.70, 144.80, 144.43, 144.17, 144.07, 142.39, 141.87, 141.45, 141.37, 138.84, 138.18, 138.01, 125.13, 124.55, 109.80, 109.62, 109.08. FAB-MS: calcd 462.10, m/z = 463.1 (M+H$^+$). Anal. Found (Calcd) for $C_{24}H_{15}AlN_6O_3$: C, 62.31 (62.34); H, 2.93 (3.27); N, 17.88 (18.17).

Synthesis of Tris(4-hydroxy-8-methyl-1,5-naphthyridinato)aluminum (AlmND$_3$). This compound was synthesized in the same manner as **AlND$_3$**, except that **mND** (1.00 g, 6.2 mmol) was used instead of **ND**. The pure product was isolated as a white solid. Yield: 86% (0.90 g). ^{1}H NMR (400 MHz, $CDCl_3$): δ 8.73−8.70 (m, 3H), 8.57 (d, 1H, J = 4.90 Hz), 8.52 (d, 1H, J = 4.91 Hz), 7.51 (d, 1H, J = 4.81 Hz), 7.42 (d, 1H, J = 4.90 Hz), 7.27 (d, 1H, J = 4.76 Hz), 7.11 (d, 1H, J = 4.94), 6.94 (d, 1H, J = 5.34 Hz), 6.91 (d, 2H, J = 5.34 Hz), 2.84 (s, 3H), 2.79 (s, 3H), 2.77 (s, 3H). ^{13}C NMR (100 MHz, $CDCl_3$): δ 165.58, 165.44, 165.12, 154.74, 154.22, 154.20, 153.22, 152.70, 152.56, 143.95, 143.76, 143.70, 143.65, 143.62, 141.75, 137.99, 137.31, 137.18, 125.25, 125.23, 124.69, 109.68, 109.40, 108.91, 17.76, 17.67. FAB-MS: calcd 504.15, m/z = 505.1 (M+H$^+$). Anal. Found (Calcd) for $C_{27}H_{21}AlN_6O_3$: C, 64.20 (64.28); H, 4.33 (4.20); N, 16.36 (16.66).

Synthesis of Tris(4-hydroxy-2,8-dimethyl-1,5-naphthyridinato)aluminum (AlmmND$_3$). This compound was synthesized in the same manner as **AlND$_3$**, except that **mmND** (0.50 g, 2.9 mmol) was used instead of **ND**. The pure product was isolated as a white solid. Yield: 86% (0.45 g). ^{1}H NMR (400 MHz, $CDCl_3$): δ 8.46 (d, 1H, J = 4.88 Hz), 8.43 (d, 1H, J = 4.88 Hz), 7.42 (d, 1H, J = 4.88 Hz), 7.34 (d, 1H, J = 4.88 Hz), 7.18 (d, 1H, J = 4.92 Hz), 7.00 (d, 1H, J = 4.96 Hz), 6.81 (s, 2H), 6.80 (s, 1H), 2.80 (s, 3H), 2.76 (s, 3H), 2.74 (s, 3H), 2.61 (s, 3H), 2.60 (s, 6H). ^{13}C NMR (100 MHz, $CDCl_3$): δ 165.03, 164.76, 164.24, 163.59, 152.01, 151.57, 151.40, 143.09, 143.05, 142.99, 142.74, 142.48, 140.61, 136.89, 136.23, 136.09, 125.08, 124.60, 109.67, 109.26, 108.89, 26.36, 26.29, 17.60, 17.53. FAB-MS: calcd 546.20, m/z = 547.2 (M+H$^+$). Anal. Found (Calcd) for $C_{30}H_{27}AlN_6O_3$: C, 65.54 (65.93); H, 4.94 (4.98); N, 15.37 (15.38).

Synthesis of Tris(4-hydroxy-8-dimethyl-2-phenyl-1,5-naphthyridinato)aluminum (AlmpND$_3$). This compound was synthesized in the same manner as **AlND$_3$**, except that **mpND** (0.20 g, 0.9 mmol) was used instead of **ND**. The pure product was isolated as a white solid. Yield: 77% (0.16 g). ^{1}H NMR (400 MHz, d_6-DMSO): δ 8.59 (d, 1H, J = 4.90 Hz), 8.49 (d, 1H, J = 4.92 Hz), 8.23−8.20 (m, 6H), 7.78 (d, 1H, J = 5.00 Hz), 7.69 (d, 1H, J = 4.91 Hz), 7.58−7.42 (m, 14H), 2.85 (s, 3H), 2.83 (s, 3H), 2.80 (s, 3H). ^{13}C NMR (100 MHz, $CDCl_3$): δ 165.79, 165.75, 165.51, 161.48, 161.04, 153.20, 152.82, 152.69, 143.43, 143.32, 143.12, 141.23, 140.46, 140.25, 139.94, 137.32, 136.68, 136.52, 129.65, 129.46, 129.29, 128.71, 128.67, 128.60, 127.72, 127.65, 127.62, 125.39, 124.88, 17.55, 17.47. FAB-MS: calcd 732.24, m/z = 733.3 (M+H$^+$). Anal. Found (Calcd) for $C_{45}H_{33}AlN_6O_3$: C, 73.84 (73.76); H, 4.37 (4.54); N, 11.37 (11.47).

Synthesis of Tris(4-hydroxy-8-methyl-1,5-naphthyridinato)gallium (GamND$_3$). To a water solution (7.2 mL) were added **mND** (0.14 g, 0.87 mmol) and gallium chloride (0.06 g, 0.34 mmol). The reaction mixture was heated and stirred at ∼40 °C. An excess amount of potassium acetate was added to the solution to change the solution acidity from pH 3−4 to pH 7−8. During the reaction (ca. 1 h), the formation of a milky white solid emitting blue fluorescence was observed. After cooling, the reaction solution was filtered to isolate the white solid. After washing with water, the solid was vacuum-dried and finally subjected to zone-temperature sublimation. The pure product was isolated as a white solid. Yield: 67% (0.11 g). ^{1}H NMR (400 MHz, $CDCl_3$): δ 8.70 (d, 3H, J = 5.36 Hz), 8.62 (d, 1H, J = 4.83 Hz), 8.57 (d, 1H, J = 4.90 Hz), 7.54 (d, 1H, J = 4.80 Hz), 7.46 (d, 1H, J = 4.71 Hz), 7.31 (d, 1H, J = 4.78 Hz), 7.27 (d, 1H, J = 4.89), 6.96 (d, 1H, J = 5.37 Hz), 6.93 (d, 1H, J = 5.42 Hz), 6.92 (d, 1H, J = 5.36 Hz), 2.84 (s, 3H), 2.80 (s, 3H), 2.78 (s, 3H). ^{13}C NMR (100 MHz, $CDCl_3$): δ 165.18, 164.98, 164.74, 154.43, 153.96, 153.51, 153.04, 153.00, 143.89, 143.81, 143.41, 143.15, 141.22, 136.08, 135.45, 135.34, 125.23, 125.14, 124.71, 109.61, 109.51, 108.97, 17.95, 17.85. FAB-MS: calcd 546.09, m/z = 547.0 (M+H$^+$). Anal. Found (Calcd) for $C_{27}H_{21}GaN_6O_3$: C, 59.03 (59.26); H, 4.00 (3.87); N, 15.09 (15.36).

Synthesis of Tris(4-hydroxy-2,8-dimethyl-1,5-naphthyridinato)gallium (GammND$_3$). This compound was synthesized in the same manner as **GamND$_3$**, except that **mmND** (0.60 g, 3.4 mmol) was used instead of **mND**. The pure product was isolated as a white solid. Yield: 83% (0.56 g). ^{1}H NMR (400 MHz, $CDCl_3$): δ 8.51 (d, 1H, J = 4.83 Hz), 8.48 (d, 1H, J = 4.86 Hz), 7.45 (d, 1H, J = 4.78 Hz), 7.38 (d, 1H, J = 4.90 Hz), 7.23 (d, 1H, J = 4.89 Hz), 7.15 (d, 1H, J = 4.90 Hz), 6.83−6.82 (m, 3H), 2.80 (s, 3H), 2.77 (s, 3H), 2.75 (s, 3H), 2.61 (s, 3H), 2.59 (s, 6H). ^{13}C NMR (100 MHz, $CDCl_3$): δ 164.63, 164.56, 164.36, 163.94, 163.40, 163.33, 152.32, 151.88, 143.31, 143.25, 142.20, 142.00, 140.07, 135.02, 134.38, 134.26, 125.10, 124.96, 124.62, 109.57, 109.32, 108.88, 26.31, 17.80, 17.71. FAB-MS: calcd 588.14, m/z = 589.0 (M+H$^+$). Anal. Found (Calcd) for $C_{30}H_{27}GaN_6O_3$: C, 61.50 (61.14); H, 4.63 (4.62); N, 14.17 (14.26).

Synthesis of Tris(4-hydroxy-8-dimethyl-2-phenyl-1,5-naphthyridinato)gallium (GampND$_3$). This compound was synthesized in the same manner as **GamND$_3$**, except that **mpND** (0.20 g, 8.5 mmol) was used instead of **mND**. The pure product was isolated as a white solid. Yield: 69% (0.15 g). ^{1}H NMR (400 MHz, $CDCl_3$): δ 8.62 (d, 1H, J = 4.88 Hz), 8.59 (d, 1H, J = 4.88 Hz), 8.15−8.12 (m, 6H), 7.53−7.40 (m, 14H), 7.33 (d, 1H, J = 5.04 Hz), 7.30 (d, 1H, J = 4.96 Hz), 2.93 (s, 3H), 2.92 (s, 3H), 2.86 (s, 3H). ^{13}C NMR (100 MHz, $CDCl_3$): δ 165.42, 165.31, 165.13, 161.13, 160.78, 160.70, 153.50, 153.15, 153.11, 143.63, 143.59, 142.77, 142.62, 140.66, 140.39, 140.19, 139.91, 135.45, 134.82, 134.70, 129.64, 129.46, 129.32, 128.69, 128.67, 128.60, 127.69, 128.61, 125.38, 125.24, 124.87, 106.99, 106.61, 106.24, 17.73, 17.65. FAB-MS: calcd 774.19, m/z = 775.2 (M+H$^+$). Anal. Found (Calcd) for $C_{45}H_{33}GaN_6O_3$: C, 69.80 (69.69); H, 4.27 (4.29); N, 10.72 (10.84).

Synthesis of Tris(4-hydroxy-8-methyl-1,5-naphthyridinato)indium (InmND$_3$). To a water solution (7.2 mL) were added **mND** (0.15 g, 0.94 mmol) and indium chloride (0.07 g, 0.32 mmol). The reaction mixture was stirred and heated at reflux temperature. An excess amount of potassium acetate was added to the solution to change the solution acidity from pH 3−4 to pH 7−8. During the reaction (ca. 1 h), the formation of a milky white solid was observed. However, the blue fluorescence from such a precipitate was barely discernible. After the removal of water by vacuum distillation, the resulting solid was subjected to Soxhlet extration by dichloromethane for 24 h. The extracted dichloromethane solution was evaporated until dryness, and the solid residue was further purified by zone-temperature sublimation. The pure product was isolated as an off-white solid. Yield: 76% (0.14 g). ^{1}H NMR (400 MHz, $CDCl_3$): δ 8.67 (d, 3H, J = 5.40 Hz), 8.33 (d, 3H, J = 4.80 Hz), 7.51 (dd, 3H, J = 4.79 Hz, J = 0.71 Hz), 6.95 (d, 3H, J = 5.41 Hz), 2.83 (s, 9H). ^{13}C NMR (100 MHz, $CDCl_3$): δ 165.73, 153.71, 153.68, 144.30, 144.22, 136.46, 125.04, 110.75, 18.23. FAB-MS: calcd 592.07, m/z = 593.0 (M+H$^+$). Anal. Found (Calcd) for $C_{27}H_{21}InN_6O_3$: C, 54.79 (54.75); H, 3.46 (3.57); N, 14.07 (14.19).

Synthesis of Tris(4-hydroxy-2,8-dimethyl-1,5-naphthyridinato)indium (InmmND$_3$). This compound was synthesized in the same manner as **InmND$_3$**, except that **mmND** (0.17 g, 0.98 mmol) was used instead of **mND**. The pure product was isolated as an

off-white solid. Yield: 81% (0.17 g). ^{1}H NMR (400 MHz, $CDCl_3$): δ 8.22 (d, 3H, J = 4.80 Hz), 7.43 (dd, 3H, J = 4.82 Hz, J = 0.68 Hz), 6.84 (s, 3H), 2.79 (s, 9H), 2.53 (s, 9H). ^{13}C NMR (100 MHz, $CDCl_3$): δ 165.19, 163.02, 152.57, 143.74, 143.04, 135.36, 124.89, 110.57, 26.15, 18.04. FAB-MS: calcd 634.12, m/z = 635.1 ($M+H^+$). Anal. Found (Calcd) for $C_{30}H_{27}InN_6O_3$: C, 56.49 (56.80); H, 4.24 (4.29); N, 12.96 (13.25).

Synthesis of Tris(4-hydroxy-8-dimethyl-2-phenyl-1,5-naphthyridinato)indium (InmpND$_3$). This compound was synthesized in the same manner as **InmND$_3$**, except that **mpND** (0.50 g, 2.1 mmol) was used instead of **mND**. However, the precipitate formed during the reaction was observed for blue fluorescence, and it was isolated by filtration. After washing with water, the solid was vacuum-dried and finally subjected to zone-temperature sublimation. The pure product was isolated as an off-white solid. Yield: 51% (0.30 g). ^{1}H NMR (400 MHz, $CDCl_3$): δ 8.34 (d, 3H, J = 4.80 Hz), 8.15−8.12 (m, 6H), 7.53−7.51 (m, 6H), 7.49−7.40 (m, 9H), 2.91 (s, 9H). ^{13}C NMR (100 MHz, $CDCl_3$): δ 165.99, 160.24, 153.78, 144.04, 143.62, 140.05, 135.77, 129.44, 128.63, 127.57, 125.15, 107.86, 17.99. MOLDI-TOF MS: calcd 820.17, m/z = 821.15 ($M+H^+$). Anal. Found (Calcd) for $C_{45}H_{33}InN_6O_3$: C, 65.78 (65.86); H, 3.95 (4.05); N, 10.26 (10.24).

Acknowledgment. This research was supported in part by the National Science Council of Taiwan, Academia Sinica, National Taiwan Normal University, National Chung Cheng University, National Taiwan University, and National Chiao Tung University.

Supporting Information Available: The synthesis and structural characterization data of chelating ligands, **ND**, **mND**, **mmND**, **mpND**, and their precursors are described. DSC thermograms of **AlmpND$_3$**, **GampND$_3$**, and **InmpND$_3$** (Figure S1); EL characteristics (Figure S2) and data (Table S1) of nondoped **GamND$_3$**, **GammND$_3$**, **InmND$_3$**, or **InmmND$_3$** OLEDs; absorption and photoluminescence spectra of **AlmND$_3$** and rubrene as well as their solution fluorescence images (Figure S3) are given. The crystallographic information is listed in Table S2 and file (.cif) also given for **AlND$_3$**·CH_2Cl_2. This material is available free of charges via the Internet at http://pubs.acs.org.

JA807284E